



DE87007753

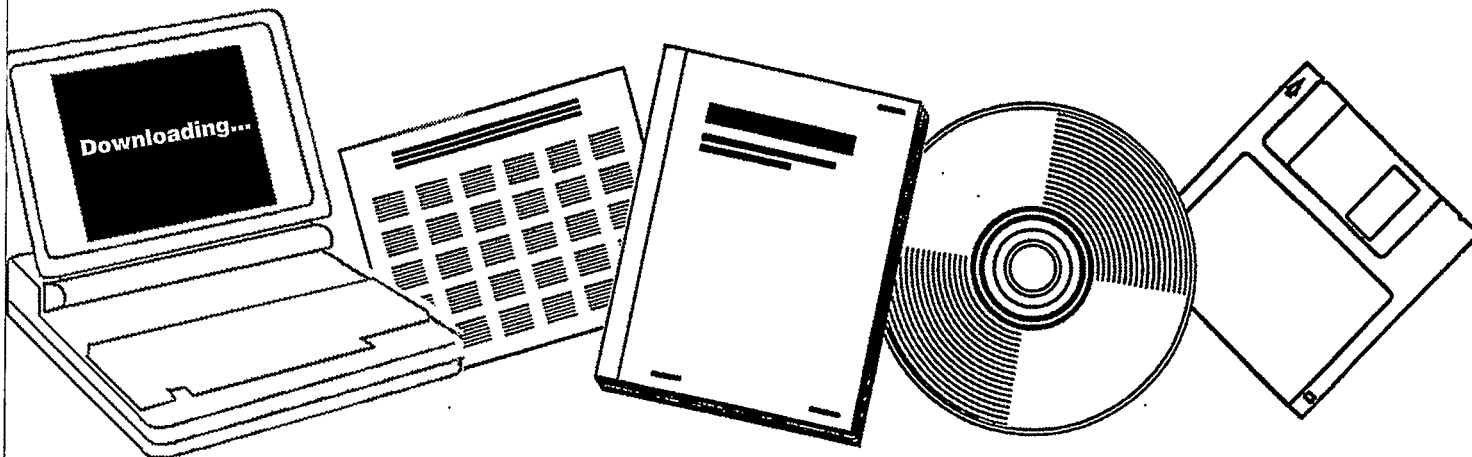
NTIS

One Source. One Search. One Solution.

METALLIC GLASSES AS NEW CATALYST SYSTEMS FOR ENERGY CONVERSION: FINAL REPORT

SOUTHERN ILLINOIS UNIV. AT CARBONDALE

1987



U.S. Department of Commerce
National Technical Information Service

DOE/ER/45122-T1

DE/FG02-84ER45122

DOE/ER/45122--T1

DE87 007753

FINAL REPORT

FOR

METALLIC GLASSES AS NEW CATALYST
SYSTEMS FOR ENERGY CONVERSION

BY

W. E. BROWER, JR.

Department of Mechanical Engineering and Energy Processes and
Molecular Science Program

GERARD V. SMITH

Department of Chemistry and
Molecular Science Program

SOUTHERN ILLINOIS UNIVERSITY

CARBONDALE, IL 62901

DISCLAIMER

This report was prepared as an account of work sponsored by an agency of the United States Government. Neither the United States Government nor any agency thereof, nor any of their employees, makes any warranty, express or implied, or assumes any legal liability or responsibility for the accuracy, completeness, or usefulness of any information, apparatus, product, or process disclosed, or represents that its use would not infringe privately owned rights. Reference herein to any specific commercial product, process, or service by trade name, trademark, manufacturer, or otherwise does not necessarily constitute or imply its endorsement, recommendation, or favoring by the United States Government or any agency thereof. The views and opinions of authors expressed herein do not necessarily state or reflect those of the United States Government or any agency thereof.

ABSTRACT

Pd-Si metallic glasses have been utilized as catalysts in the Fischer-Tropsch reaction. The glasses are selective of ethane, whereas the in-situ crystallized glasses select a range of hydrocarbons characteristic of conventional Pd catalysts. This shift in selectivity has been observed in other hydrogenation reactions. Surface crystallization caused by the reaction conditions causes variable selectivity. Crystallization in reaction conditions has been monitored by DSC.

During the course of the grant we developed the use of (+)-apopinene (6,6-dimethyl-1*R*,5*R*-bicyclo[3.1.1]hept-2-ene) as a molecular probe for determining the number and kinds of active sites on metallic glass catalysts. To accomplish this we conducted many experiments for comparison on other types of catalysts. These were foils, powders, and highly dispersed metals on several different supports. The glassy surfaces appear to be three dimensionally random (hilly or rolling) with many protuberances which crystallize into staircases of steps and kinks.

	<u>Contents</u>	Page
I.	Abstract	2
II.	Contents	3
III.	Results and Discussion	5
	A. Surface Analyses of Metallic Glass Catalysts	5
	1) Computer Simulation	5
	a. Bulk Model Generation	7
	b. Surface Model Generation	9
	c. Results	14
	d. Discussion	16
	e. Conclusions	19
	f. References	20
	2) HVEM at Argonne National Laboratory	21
	a. Experimental Procedure	22
	b. Results	23
	i. Vacuum Aging	23
	ii. Cyclohexane Aging	24
	c. Discussion	25
	d. Conclusions	27
	e. References	27
	3) Ion Scattering Spectroscopy	28
	a. Conclusions	32
	4) Conversion Electron Moessbauer Spectroscopy	32
	a. Introduction	33
	b. Experimental Procedure	34
	c. Results and Discussions	34
	d. Conclusions	36
	B. Bulk Analyses	36
	1) Moessbauer Spectroscopy	36
	2) DSC/DTA - 8ICC	37
	3) References	38
	C. RSM Processing - Splat Forming Methods	39
	1) Hammer and Anvil Discs	39
	2) Shock Tube Flakes	39
	3) Single Roller Quenching	39
	D. Catalytic Measurements	40
	1) Fischer-Tropsch Reaction	40
	a. References	44
	2) Boudouard Reaction	45
	a. Supported Nickel	45
	b. Metallic Glasses	46
	c. References	46

3)	Characterization of Metallic Glass Catalysts with the Sterically Complex Molecular Probe (+)-Apopinene	47
a.	The Method for Using (+)-Apopinene for Characterizing Surfaces	47
b.	Hydrogenation of (+)-Apopinene over Metallic Glasses	48
c.	The Characterization of Pt Catalysts with (+)-Apopinene	49
d.	The Characterization of Pd Catalysts with (+)-Apopinene	50
e.	References	50
E.	Publications and Presentations	51
	1) Publications	51
	2) In Press - preprints enclosed	52
	3) Presentations	52
F.	Theses	55
G.	Personnel	56

I. Results and Discussion

A. Surface Analyses of Metallic Glass Catalysts

1. Computer Simulation

Much work has been done in recent years concerning the characterization of glassy metals. Computer generated models of the bulk structures of metallic glasses have been described which successfully predict density, and whose model generated radial distribution functions fit experimental results from neutron diffraction and EXAFS. The atomic scale bulk structure has been modelled by a dense random packing of hard spheres [1] and by the sequential addition of single atoms to different seed structures [2]. Clear improvement to the fit of the radial distribution functions to experimental results was obtained by Barker when the resulting configurations were allowed to relax under the influence of a simple potential energy function [3].

One way to characterize the roughness of the surface is to introduce the fractal dimension [4], $D = \frac{\log N}{\log 1/r}$, where $N = \alpha^2$, $r = 1/\alpha$, and α is the number of subsegments, and r is the length of the segment. For example, a Brownian Island, which represents random walk, has a dimension $D = 2.30$.

The metal-metalloid type of glassy metal exhibits some unique features. It was found from EXAFS experiments that each metalloid has a constant number of metal near neighbors [5]. This suggests that the metalloid sites form the center of some kind of molecular unit, which is characteristic of the alloy system. This idea was proposed by Gaskell [6], who analyzed the bulk structure of Pd_4Si glass constructed by packing NM_6 trigonal prisms (N-metalloid atoms, m-metal atoms).

Only a little work has been done in the characterization of the surface of metallic glass. The first attempt was by S. M. Garofalini [7], whose model dealt with a theoretical single component amorphous material. The distribution of the binding energies of the surface atoms was found. This distribution indicates the presence of a high density of high binding energy sites, which were similar to those expected for adatoms at kink sites on closed-packed surfaces. The energy profile of a diffusing surface atom and the binding energies of surface atoms indicate that the surface of amorphous solids are rough. However, an alloy glass exhibits chemical SRO, which does not exist in Garofalini's model. Thus, Garofalini's model is not suitable to describe the surface of an amorphous metallic glass alloy.

In the case of crystalline materials, the TLK model shown in Figure 1 is well known. The surface according to this model has a high density of sites with coordination number 9 on the terraces (A-site), and a lower density of low coordinated sites: ledges (B-site), kinks (C-site), and adatoms (D-site). This work presents a computer simulation technique employed to study the surface characteristics of Pd_4Si alloy metallic glass in terms of distribution functions of surface atom coordination numbers. These distributions will be compared to those generated from surfaces which occur on crystalline Pd, which fit the TLK model, Figure 1 and to small crystalline particles, similar to supported metal catalysts.

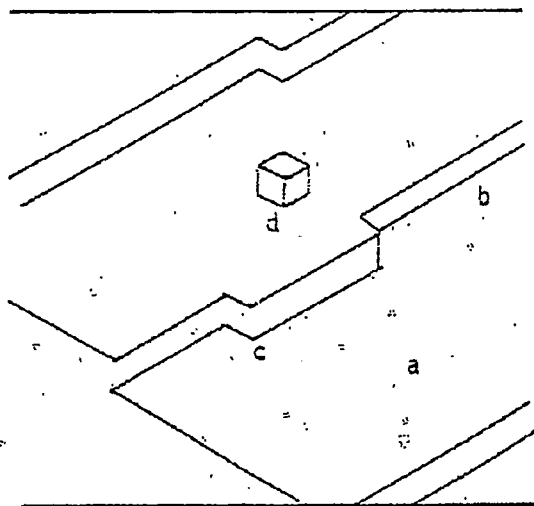


Figure 1. Terrace-Ledge-Kink (TLK) model showing the following sites: terrace a-site, ledge b-site, kink c-site and adatom d-site.

a. Bulk Model Generation

The computer generation procedure in this work is similar to Gaskell's bulk model for Pd_4Si glass [6]. The NM_6 trigonal prism was chosen to form the basic structural unit of the bulk glass structure (Figure 2). The six palladium atoms are at the corners of the trigonal prism and the silicon atom is put at the center of the prism. Gaskell's trigonal prism, Fig. 2a, has a void of a radius 0.725 Å. Thus, in Gaskell's case, putting silicon atoms (1.117 Å radius) inside the voids caused severe distortion of the prism. In our case the prism is such that it initially contains the silicon atom. Gaskell's trigonal prism is shown in Figure 2a, and our modified trigonal prism is shown in Figure 2b. The next units are related to the original prism by clockwise rotations through $221^\circ 12'$ around the axis in the same plane, while in Gaskell's case the rotation was 215.3° . Repeated rotations around the axis in the same plane produce the edge-sharing arrangement of trigonal prisms. The larger rotation angle in our model to produce edge sharing was necessitated by the expanded trigonal prism as compared to Gaskell.

The result of starting with a trigonal prism and generating the bulk structure by repetitive rotations is shown in Figure 3a, a 78 atom wooden ball model. The presence of silicon atoms in the prism causes more artificial voids, Figure 3a, than that depicted by Gaskell, whose prisms were empty initially. A bulk structure is built up in our computer model by adding successive layers of trigonal prisms to the original trigonal prism until 860 or 1200 total atoms have been added. This procedure is continued until the most dense packed arrangement of trigonal

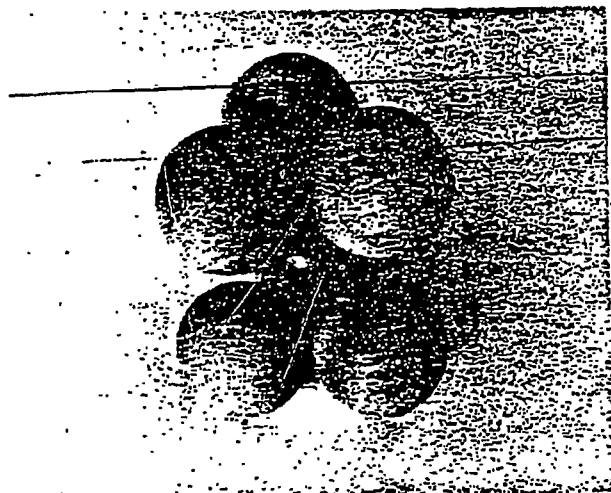
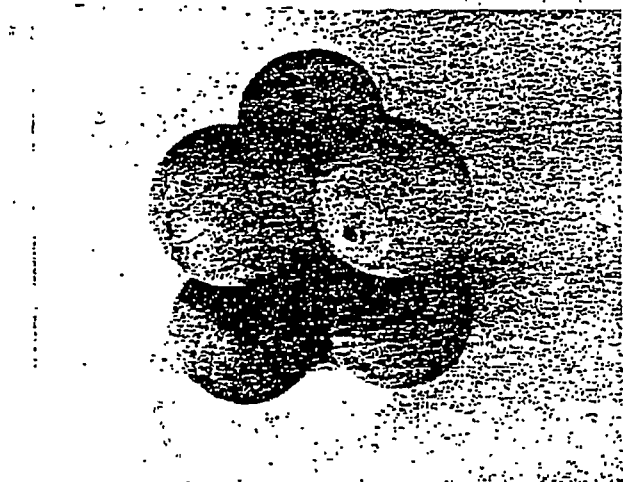


Fig. 2. The trigonal prism used on the bulk simulation procedure
a) Gaskel (5) b) this work.

prisms is reached. The generating procedure maintains the NM_6 short range order, while packing the trigonal prisms as efficiently as possible. At each trigonal prism addition step, the whole structure is checked for overlapping. If there is an overlapping, the addition of the whole the prism does not proceed and, as a result of this, artificial voids appear.

At this stage the model is not adequately physical and needs a bulk relaxation procedure. This goal was accomplished by minimizing the internal energy. The cohesive energy of such a system was assumed to be adequately represented by a sum of pairwise interactions [8]. For the present work a 6-12 Lennard-Jones potential was chosen. The interatomic potential $V_{ij} = 4 \epsilon_{ij} \left[\left(\frac{R_{ij}^0}{r_{ij}} \right)^{12} - \left(\frac{R_{ij}^0}{r_{ij}} \right)^6 \right]$, where $R_{ij} = 2^{-1/6} R_{ij}^0$, and r_{ij} is the distance between atoms i and j and R_{ij}^0 is the equilibrium interatomic distance. The quantity ϵ_{ij} is the binding energy between atoms in i and j which is assumed to be equal to cohesive energy. The explicit form of this potential for our system is given by the following equations where values of ϵ_{ij} and R_{ij} for Pd and Si are taken from Boudreaux [8]:

$$V_{Pd-Pd} = 1.96 \left\{ \left[\frac{2^{-1/6} \times 2.77}{r} \right]^{12} - \left[\frac{2^{-1/6} \times 2.77}{r} \right]^6 \right\} \quad (1)$$

$$V_{Pd-Si} = 2.73 \left\{ \left[\frac{2^{-1/6} \times 2.47}{r} \right]^{12} - \left[\frac{2^{-1/6} \times 2.77}{r} \right]^6 \right\} \quad (2)$$

$$V_{Si-Si} = 0.55 \left\{ \left[\frac{2^{-1/6} \times 2.65}{r} \right]^{12} - \left[\frac{2^{-1/6} \times 2.65}{r} \right]^6 \right\} \quad (3)$$

Compared to Boudreaux's potential terms [8], the above

potentials do not include terms due to truncation and in our case the total energy, E_t , was calculated taking into account all atoms in the model,

$$E_t = \frac{1}{2} \sum_{i,j}^N V_{ij} \quad (4).$$

The energy minimization was accomplished by steepest descents method [9]. Each atom is simultaneously moving along the direction of the net force on that atom [9]. The atoms are moved a distance proportional to the magnitude of the force on them. After each such move, the forces are recalculated and the atoms moved again. The force on atom i is given by $F_i = -\nabla V$. The atoms are then moved according to $x_{i,n} = h_i \nabla V_n$.

The constant h was chosen for each step separately. The values of h in this study were 0.1 to 1.0. The new set of coordinates in the n th interaction $x_{i,h} = x_{i,0} + \Delta x_{i,h}$. The new value of energy is calculated in new coordinates. To assure that the minimum of the total energy is reached the average force:

$$F = N^{-1} \left(\sum_{k=1}^N F_k^2 \right)^{1/2} \quad (5)$$

was introduced, where N is the total number of atoms in the model. The procedure is stopped when $F < \frac{\epsilon}{R_c}$ which assures that the final energy E_t is approached within 1% of the minimum value.

b. Surface Model Generation

The task of this work is to generate a surface of an amorphous material corresponding to the solid-vacuum interface and a solid adsorbate interface. The surface of the alloy glass was generated by two approaches, one as smooth as possible and the other as rough as possible. The smoothest possible unrelaxed

surface was generated in the following way. The boundary condition in the Z direction is imposed such that no atom is allowed to have the Z-component greater than a fixed number, Figure 3b. This boundary condition is the equivalent of a fracture surface at the dashed line in Figure 3b. This generation procedure allows composition to be maintained up to the prism layer below the top surface. In other words, up to the surface, the structure consists of trigonal prisms which generate the bulk composition $\text{Pd}_{80}\text{Si}_{20}$ utilizing a total of 860 atoms. By allowing the surface top layers to be formed without retaining the trigonal prism structure, the silicon atoms are preferentially exposed to the surface. A rough surface boundary condition was generated by simply continuing the trigonal prism structure up to the surface; utilizing a total of 1200 atoms, and preferentially exposing palladium atoms. These two boundary conditions impose a thickness range on the surface layer between atom (a total of one atom), Figure 3b, and 1 trigonal prism (a total of two prisms), Figure 3a. The minimum roughness is the amorphous equivalent of a crystallographic plane with an adatom and a vacancy, and appears to be a reasonable minimum. The maximum of one trigonal prism would appear to be a reasonable limit for metal-metalloid glasses, whose density approaches a dense random packed liquid.

The equilibrium surface segregation was finally reached by utilizing minimization of binding energy as the driving force for segregation, while neglecting the effect of entropy. The entropy contribution to the total free energy can be shown to be



Figure 3. Ball model representing: a) bulk simulation used to generate the rough surface, b) dashed line represents the smooth surface boundary condition. Both conditions correspond to the unrelaxed case.

negligible in the following way. The total free energy for the system can be formulated as follows:

$G_t = H_t - TS_t$. The pressure - volume term in enthalpy is assumed to be negligible, and instead of enthalpy we can consider the internal energy:

$G_t = E_t - TS_t$. The binding energy between the atoms in the various pairs of atoms is expressed in terms of L-J potential. For our system containing 860 atoms, the corresponding total energy was found to be $E_t = -2236$ eV after the final relaxation. The driving force of surface segregation is the minimization of the total free energy of the alloy system at a given bulk composition. The segregation can be visualized as an exchange reaction:



The entropy contribution to the total free energy,

$$S_t = [S_A(\text{surf}) + S_B(\text{surf}) + S_A(\text{bulk}) + S_B(\text{bulk})] \quad (7)$$

Only the entropy of mixing $S_A = kx_A \ln a_A$ is considered, since, in an alloy system, this term is the most important with respect to segregation. For the ideal case $S_A = kx_A \ln x_A$. Thus,

$$S_t = k(x_{\text{Pd}}^{\text{S}} \ln a_{\text{Pd}}^{\text{S}} + x_{\text{Si}}^{\text{S}} \ln a_{\text{Si}}^{\text{S}} + x_{\text{Pd}}^{\text{b}} \ln a_{\text{Pd}}^{\text{b}} + x_{\text{Si}}^{\text{b}} \ln a_{\text{Si}}^{\text{b}}) \quad (8)$$

In ideal case,

$$S_t = k(x_{Pd}^s \ln x_{Pd}^s + x_{Si}^s \ln x_{Si}^s + x_{Pd}^b \ln x_{Pd}^b + x_{Si}^b \ln x_{Si}^b), \quad (9)$$

where x_i is the concentration of i -th element, and a_i is the chemical activity of i -th element.

By assuming ideal entropy, equation 9, the entropy contribution per atom for the smooth boundary condition was found to be -1.57×10^{-16} erg/ $^{\circ}$ K at 300 $^{\circ}$ K, TS per atom was found to be -4.7×10^{-14} erg = -2.9×10^{-2} eV. Thermodynamic data provided by Kozlov et al [10] for the Pd-Si system enable correct calculations of entropy from equation 8 for the non-ideal case. The entropy contribution per atom was found -2.2×10^{-16} erg/ $^{\circ}$ K, so that at 300 $^{\circ}$ K, TS per atom is -6.6×10^{-14} erg (-4.1×10^{-2} eV). The binding energy per atom is -2.5 eV. The contribution of enthalpy per atom is almost 100 times greater than the entropy contribution at room temperature; thus, we can justify using only the energy term in the relaxation procedure. The final relaxed composition of the Pd₈₀Si₂₀ alloy for the first surface layer is Pd₆₅Si₃₅, as determined by the energy minimization calculation.

In the second approach to generating the surface structure, an initially rough surface was obtained by the last trigonal prism layer when 1200 rough atoms were exhausted, Figure 3a. This procedure generated a surface with almost the bulk composition. Many Pd atoms were at prism corners where their coordination number is three (analogous to a large population of adatoms on a (111) plane of fcc). This resulted in a very-low coordination number on relaxed surface, C.N. = 4.86. Again, the whole bulk and surface of the initial model were subjected to the L-J potential and relaxed in the same procedure as in the first

approach, the different surface generation procedure resulting in 1200 total atoms. The surface was assumed to be segregated and relaxed when the forces acting on the surface atoms are negligible ($E_t - E_{tmin}/E_{tmin} < 1\%$) and the effect of entropy in this approach was again assumed to be negligible. The final composition of the first layer was 35% of Si and 65% Pd in our first approach, and 38% Si and 62% Pd in this second approach. The dispersion (surface atoms/total atoms) was 0.24 in the second approach and 0.36 in the first approach, since there are more total atoms in the second approach, which causes dispersion to go down.

The bulk density of the model generated structure was found to be 10.1 g/cm^3 for the smooth surface approach. The system is composed of 172 silicon atoms and 688 paladium atoms. The total mass $m = 129 \times 10^{-21} \text{ g}$. The total volume of the model, $V = 128 \times 10^{-22} \text{ cm}^3$. Thus, $\rho = 10.1 \text{ g/cm}^3$ with $\Delta\rho = 0.3$ as compared to an experimental value 10.3 g/cm^3 [11], which is within experimental error.

The model volume was calculated by finding the maximum values of x , y and z which defined the model's boundaries. The volume is $33A \times 30A \times 13A = 128 \times 10^{-22} \text{ cm}^3$. The total error in the calculated volume, arising from a $0.6A$ uncertainty in the z plane, is 5%, which gives a 0.25 g/cm^3 error in the density. Since the difference between the experimental and calculated density value is 0.2 g/cm^3 , we can conclude that the relaxation of the model was accomplished within the expected error of the calculations. The discrepancy is due to the fact that even the relaxed structure has some voids, which

would lower the density value.

c. Results

Based upon this model, probability distributions of the number of nearest neighbors, C.N., for the atoms located on the surface were calculated and are plotted in Figure 4. Three types of distributions were analyzed, each of which describes the vicinity of the palladium atoms on the surface. Figure 4a shows the distribution of Pd-Pd neighbors for the surface. The distribution was calculated at the distance 2.78Å from the original atom. This distance corresponds to the first plateau position in the Pd-Pd C.N. distribution function, Figure 5b, which corresponds the first coordination shell. Figure 4b shows the distribution of Pd-Si nearest neighbors, calculated at the distance 2.57Å from a Pd atom at the origin, which corresponds to the sharp plateau in Pd-Si C.N. distribution, Figure 5a. Figure 4c shows the vicinity of Pd surface atoms for both Pd and Si neighbors with the range of C.N. from 4 to 11. The sites with C.N. 10 and 11 have very low probability. An average coordination number was C.N. = 5.94, as compared to 6.24 found in unrelaxed case, which is shown in Figure 6, analogous to Figure 4c.

The surface segregation of silicon with respect to different C.N.'s of surface sites is illustrated in Table 1. The ratio between silicon and palladium atoms for a given surface site decreases as the C.N. increases, thus showing the tendency of silicon atoms to segregate preferentially at low coordinated sites. The relaxation of the model shows that the surface is further enriched in silicon, Table 1. By using a surface

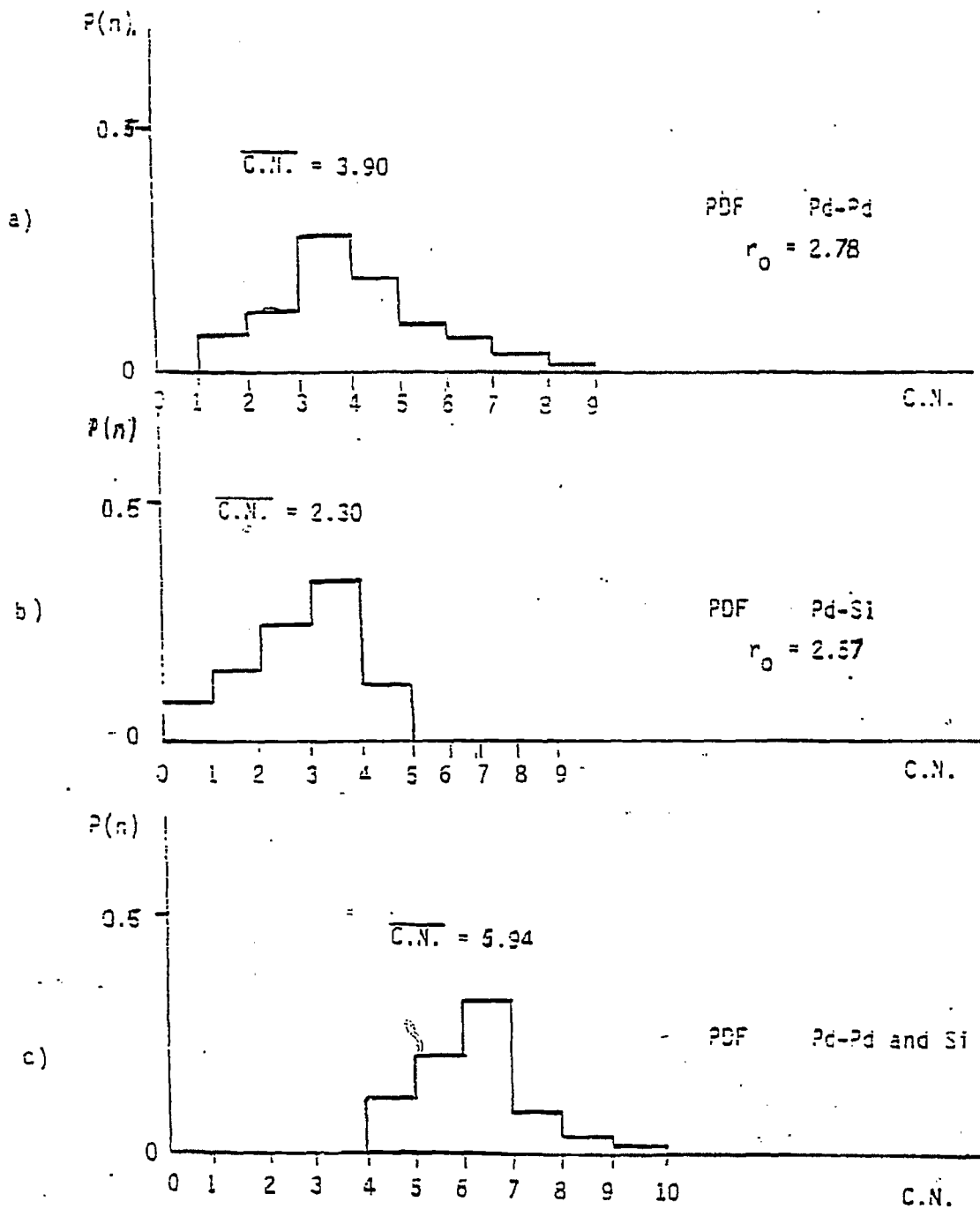


Figure 4. Probability distributions of the number of near neighbors in model of Pd₄Si glass alloy for atoms located on surface. Relaxed form of smooth boundary condition surface.

- a. Pd-Pd distribution
- b. Pd-Si distribution
- c. Combined Pd and Si distribution

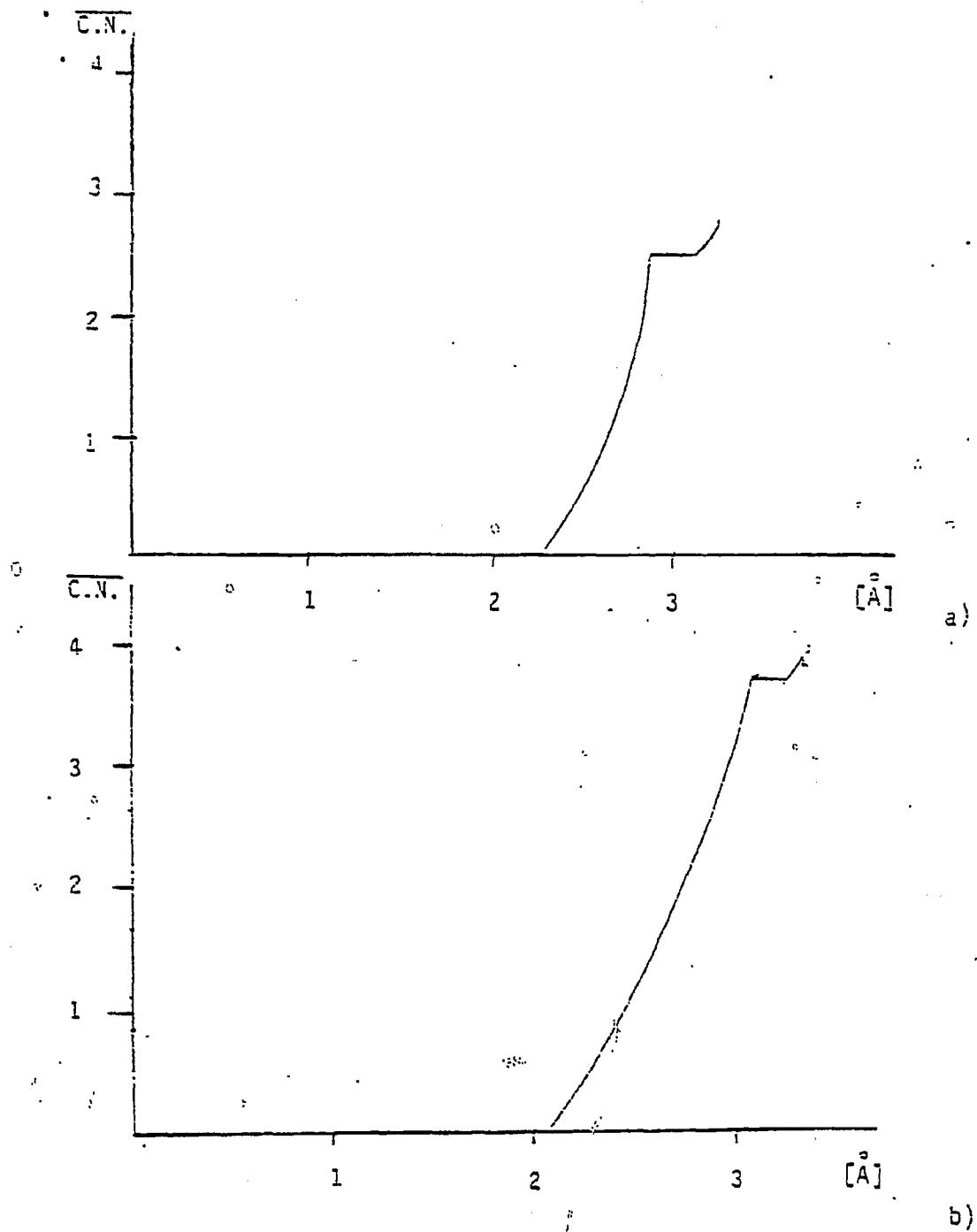


Figure 5. The average C.N. distribution for relaxed structure from smooth boundary-condition as a function of distance. The plateaus define the first coordination shell. a) Pd-Si, b) Pd-Pd

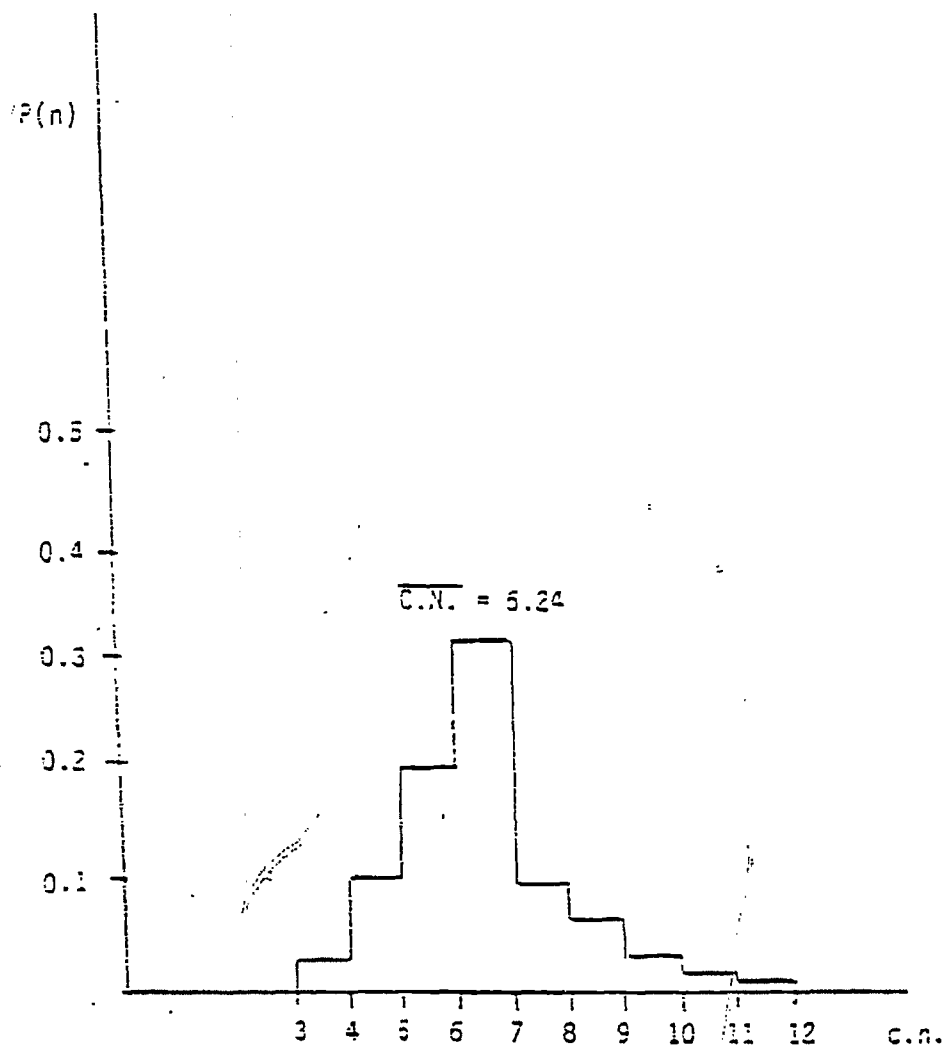


Figure 6. Probability of the number of near neighbors in the unrelaxed Pd_4Si model by assuming the smooth boundary condition initial surface.

graphics system the simulated unrelaxed surface is shown in Figure 7. The simulated surface of the relaxed and segregated glass is indistinguishable from Figure 7. The picture illustrates the roughness of the surface in terms of predominantly low coordinated sites. The roughness of the surface was described by the use of the fractal dimension, D . For the surface depicted in Figure 7, $D = 2.31$, as compared to 2.30 for the Brownian surface [4]. D was determined by how many initial squares can be found in the rectangles obtained from the surface simulation. In our case we assume that a rectangle becomes a square when $a_2 \geq 1.5(a_1)$, which leads to an error of 4% in D , or $D = 2.3 \pm 0.09$.

At this stage surface reconstruction is induced by changing the length of the bond between the atoms on the surface first layer and the bulk compared to the bulk length. The R_0 parameter in the Lennard-Jones potential for the surface atoms is reduced compared to the bulk and the scaling is directly proportional to the C.N., i.e., the smaller the coordination number, the larger the contraction. The Pd-Pd surface average coordination number distribution function exhibits a sharp peak at 2.72A from the origin atom, Figure 5b (initially 2.78A, Figure 4a) and the Pd-Si pair distribution function exhibits the first peak at 2.45A, Figure 5a (initially 2.57A, Figure 4b). These shifts in peak positions, eg. 2.78A to 2.72A, would be difficult to verify experimentally. However, the effect of such surface reconstruction on the properties of the glass is significant, as evidenced by clear shifts in catalytic selectivity which occur upon reconstruction of crystalline catalysts [18].

A similar distribution of nearest neighbors on the reconstructed surface is shown in Figure 8, which shows that only the Pd-Si distribution is changed. The effect on silicon segregation is shown in Table 1. The segregation of silicon is greatly enhanced at low coordinated sites, which is in agreement with Somorjai [12].

The model first represented the glass-vacuum interface. The model was then used to characterize the influence of physisorption on the surface structure. The physical adsorption of helium was achieved by minimizing the binding energy of the surface interacting with helium atoms. After a relaxation of the surface induced by interaction with helium atoms, the Pd-Pd pair distribution exhibits the first peak at 2.74Å and the Pd-Si distribution at 2.48Å. Surface contraction is slightly reduced by the presence of a physisorbed layer of He. The nearest neighbor distributions are shown in Figure 9.

In the second approach, using the rough boundary condition, the generated surface was rougher compared to the first approach with the CN = 5.64. This approach generated a surface graphics simulation which is indistinguishable from Figure 7. The distribution function corresponding to this case is shown in Figure 10a. The C.N. for unrelaxed model was 4.86. The corresponding distribution function is shown in Figure 10b.

d. Discussion

A description of the metal-metalloid alloy glassy surface was accomplished by examining the distribution of surface coordination numbers. The comparison is made among a single crystal surface, the surface structure of small particles, and

TABLE 1

C.N.	4	5	6	7	8	9
a) $\frac{Si}{Pd}$	0.95	0.93	0.90	0.55	0.45	0.28
b) $\frac{Si}{Pd}$	1.05	0.96	0.95	0.50	0.42	0.28

The relation between coordination numbers and segregation of silicon⁴ for (a) the model relaxed from the initially smooth surface (b) the segregated and relaxed model.

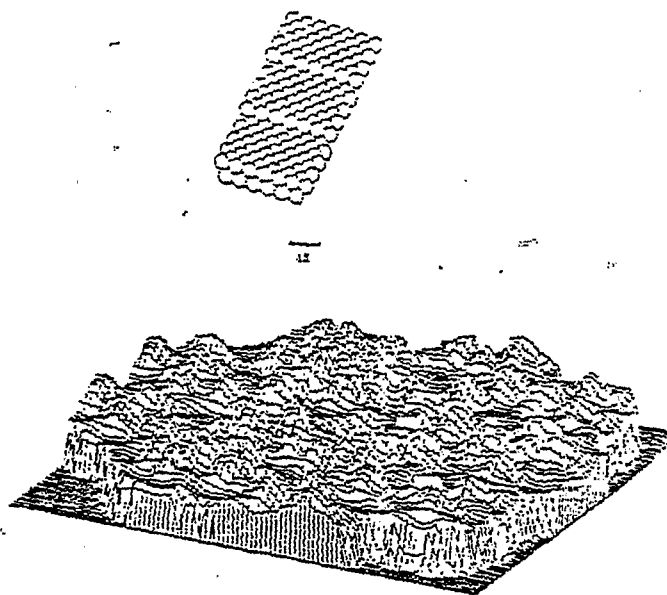


Figure 7. The surface of the relaxed Pd₄Si metallic glass displayed via graphics system as compared to stepped single crystal surface. Balls representing atoms in the single crystal surface are 2Å in diameter in the scale of this picture as compared to 2.75Å of palladium atoms and 2.23Å of silicon atoms. Smooth surface boundary condition.

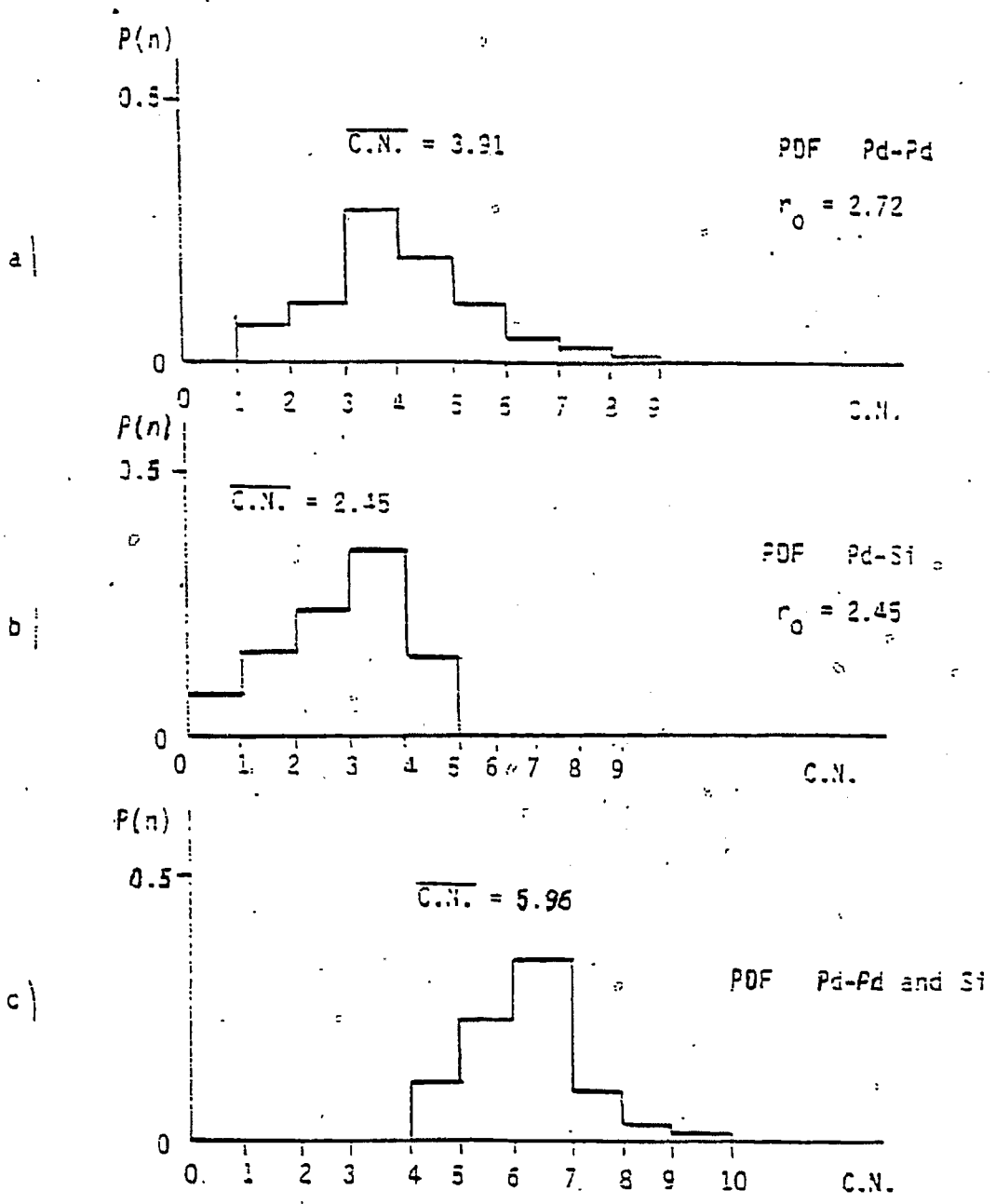


Figure 8. Probability distribution of the number of near neighbors Pd_4Si reconstructed model for relaxed form of smooth initial boundary condition surface.

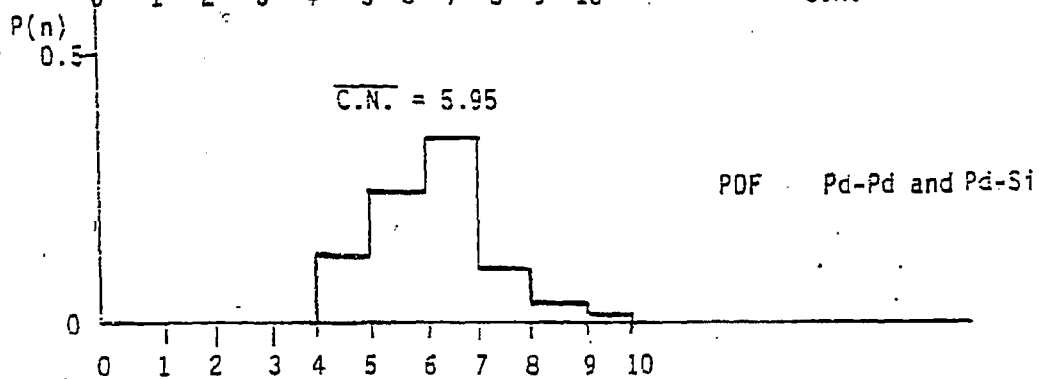
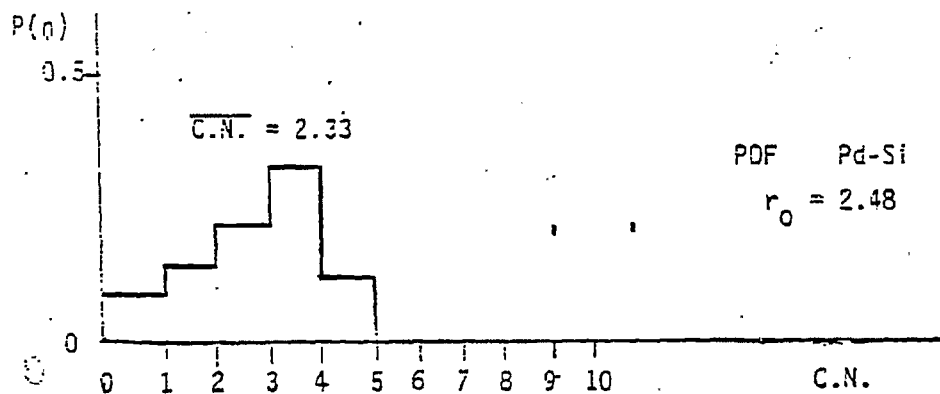
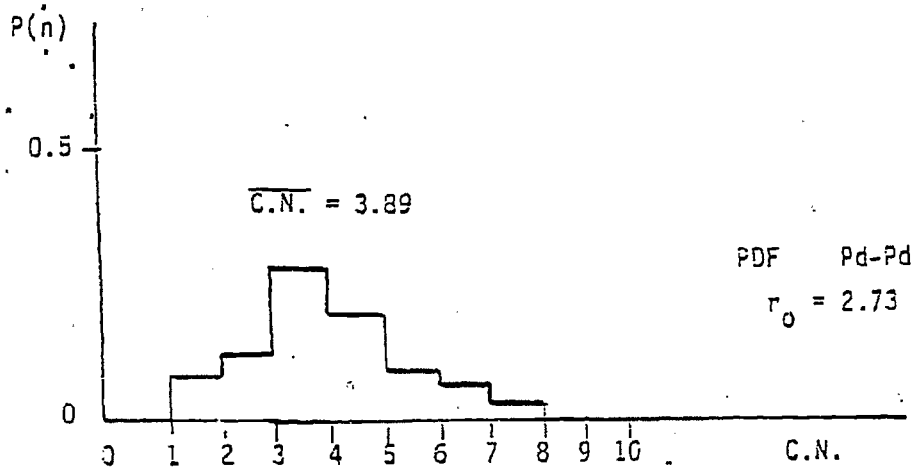


Figure 9 Probability of the number of near neighbors in Pd_4Si model for Pd atoms located on surface of Figure 8 with a physisorbed helium layer.

- Pd-Pd distribution
- Pd-Si distribution
- Combined Pd and Si distribution

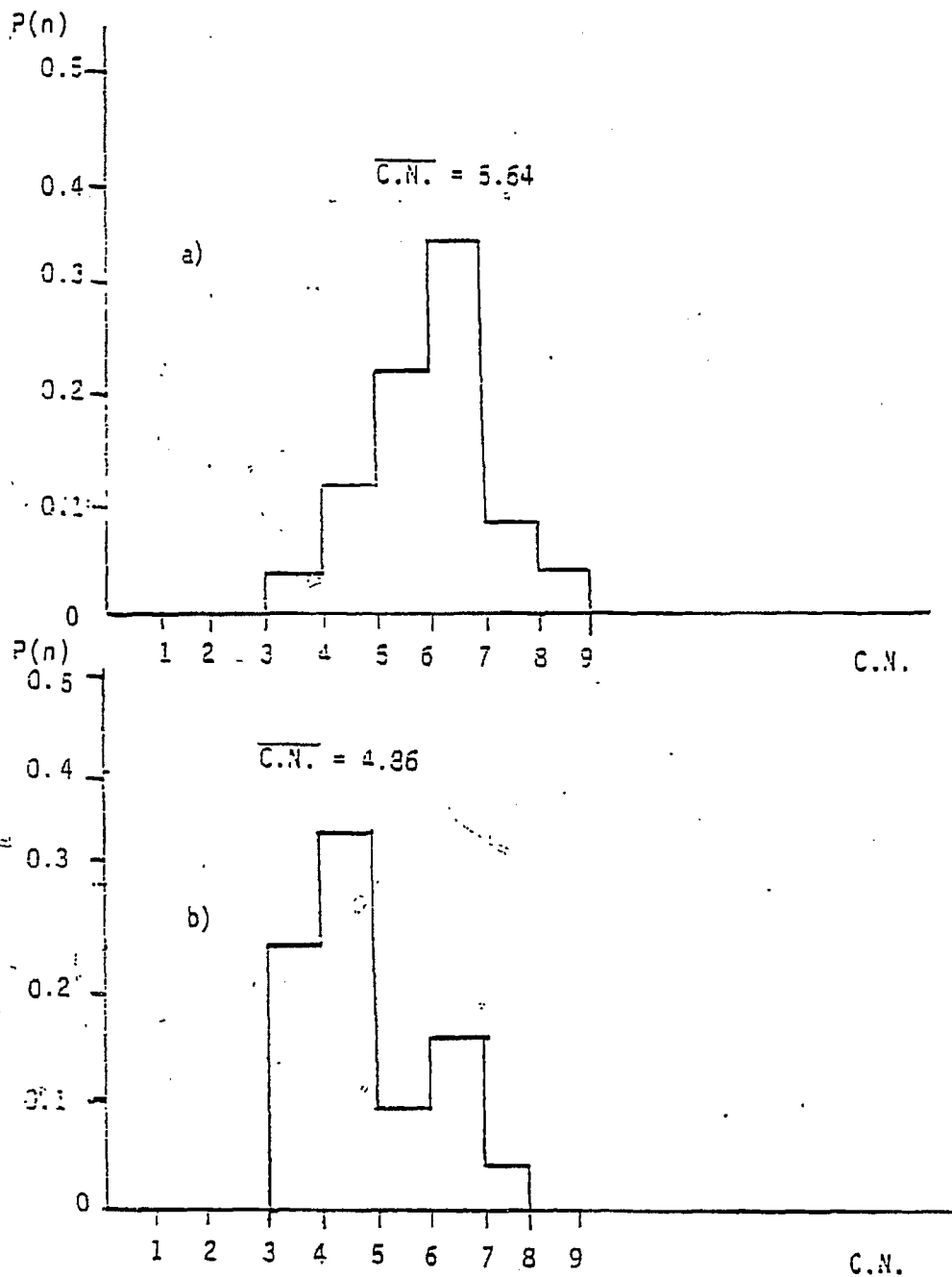


Figure 10. Probability of the number of near neighbors in Pd_4Si model by assuming the rough surface boundary condition for Pd atoms a) after relaxation b) before relaxation.

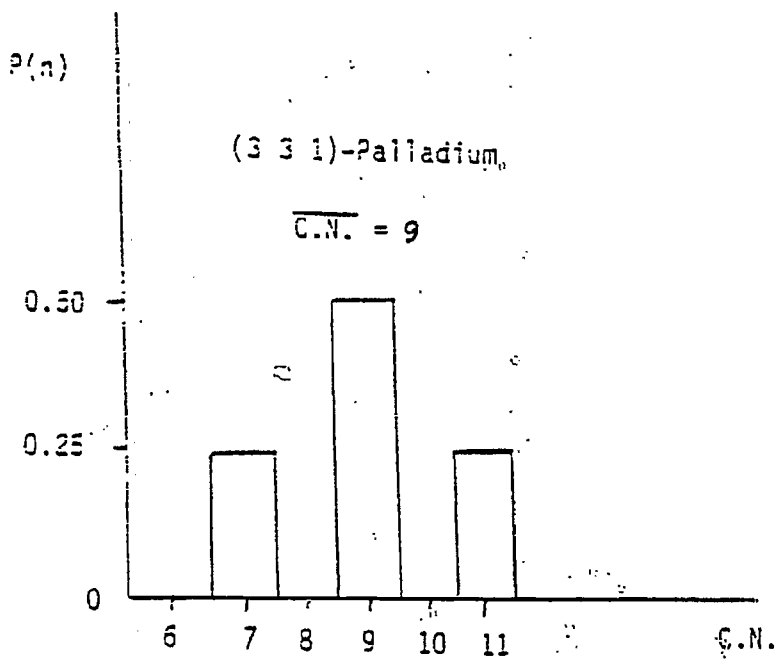
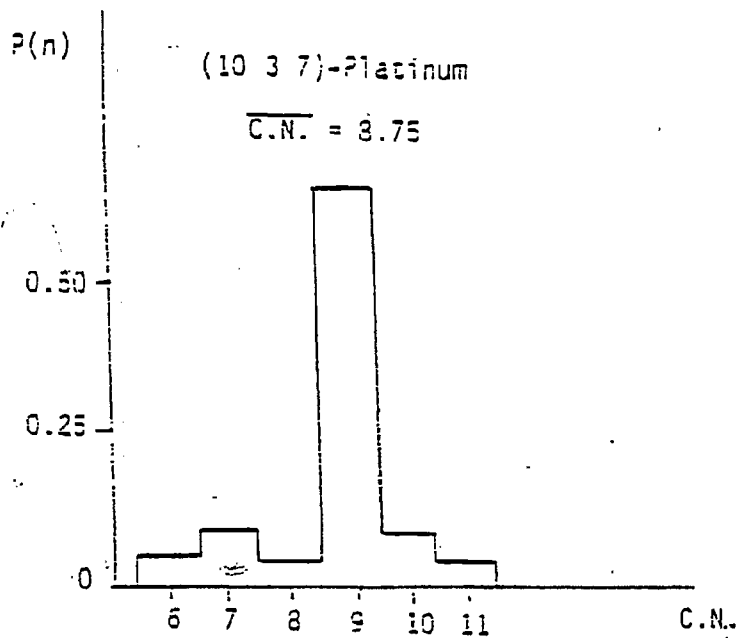


Figure 11. Coordination Number distribution functions for crystalline planes: a) (10 8 7)-Platinum b) (3 3 1) - Palladium

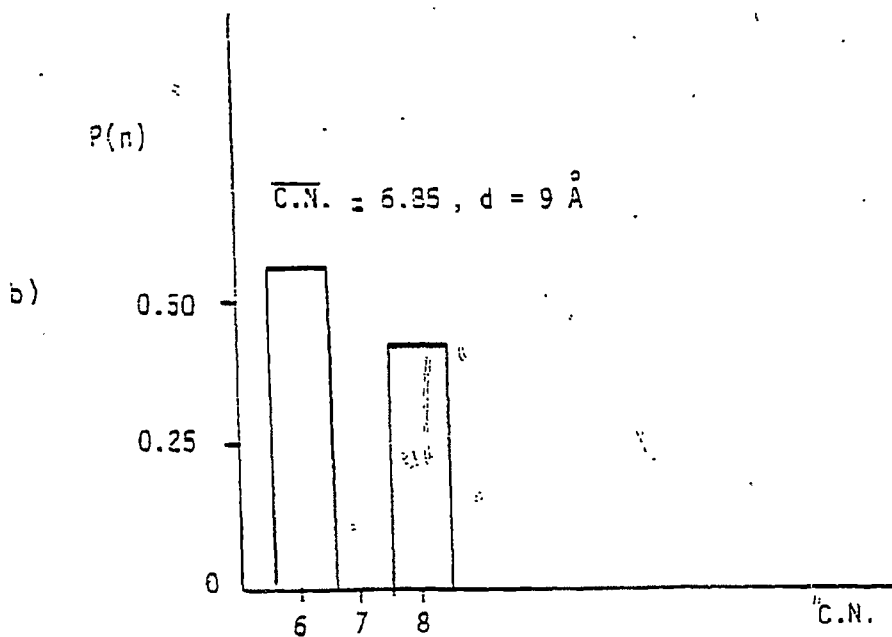
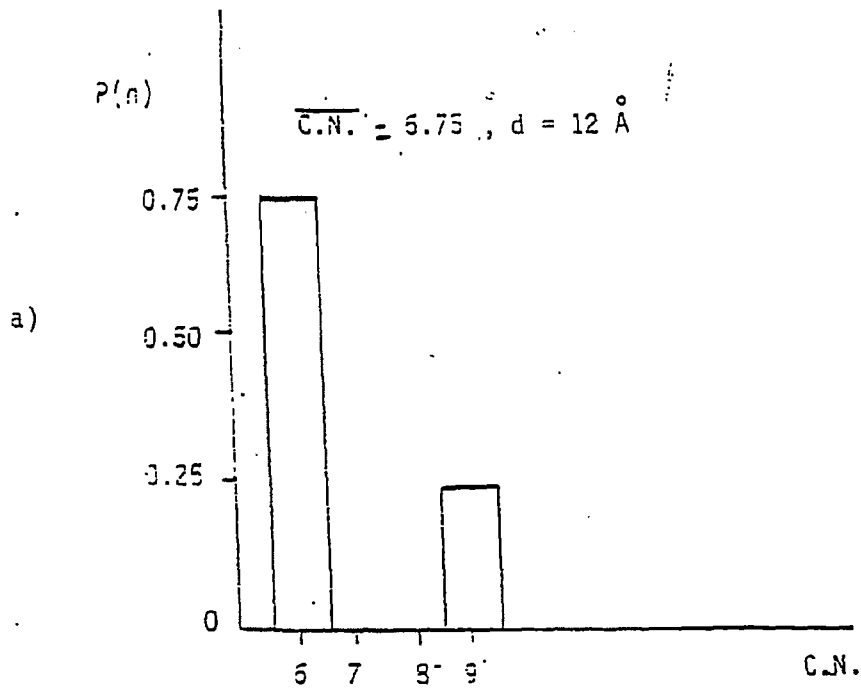


Figure 12. Surface atom coordination number distribution functions for small clusters: a) cubo-octahedral, b) fcc

the metallic glass surface model presented in this paper. From our model the C.N. distribution ranges from 4 to 11 and the mean value is about 6. One type of high Miller index plane, the (331) plane of palladium, is thermodynamically stable [13]. The distribution for surface coordination numbers for this plane is given in Figure 12b. It shows the existence of sites with coordination numbers 7, 9 and 11, but the mean value is 9, the same as on (111) plane. A kinked-stepped reconstructed surface for the (10 8 7) plane was reported stable for platinum [13]. In this case the C.N. ranges from 6 to 11, but C.N. = 8.5 (Figure 11a), close to that for an fcc (111) terrace where C.N. = 9. In case of small particles, Gillet [14] reported that for 20 Å Pd particles, the fcc structure prevails. Figure 12b shows that the distribution function has C.N. = 6.85 for the fcc particles surface atoms. Gallezot [15] reported that for platinum particles under the influence of H₂ chemisorption, a normal fcc bulk structure exists. The comparison of C.N. shows that the small particle value of C.N. = 6.85, much closer to the calculated glass value in this work of 5.96 than the highly stepped-kinked (10 8 7) platinum surface.

The small particles can have a distribution ranging only from 6 to 9, in the cube-octahedron case and the fcc case, Figure 11, since no concavities are present. The (10 8 7) surface has a wider distribution, ranging from 6 to 11, since concavities are present (C.N. = 10, 11), but no convexities are present (C.N. = 3 to 5); only the glass has a distribution ranging from 4 to 11. It may be that with respect to catalytic applications, the glass can compete with small particles for reactions which require low

coordinated sites and with the high-Miller indexed single crystal stepped surfaces for reactions, which require high-coordinated sites. This makes the glass surface very versatile for catalytic applications. It was found by Ledoux [16] that the presence of low C.N. sites on a kinked-stepped surface can account for the mechanism of olefin hydrogenation on transition metal surfaces. The selectivity of addition greatly depended on the presence of low coordinated sites. The reaction of olefins on Pd_4Si glass carried out by Brower et al [17] showed a high selectivity for addition, thus supplying further evidence that the glass surface has a high density of low coordinated sites.

The surface segregation illustrated in Table 1 shows that the segregation takes place preferentially at sites with low coordination number. Thus the composition of the surface of the $\text{Pd}_{80}\text{Si}_{20}$ alloy is enriched in silicon especially at low coordinated sites. Because, on a real surface, contraction takes place, reconstruction of the surface is necessary. This contraction is a function of coordination numbers [12]. The distribution functions show that a slight contraction is introduced to the reconstructed surface. Only the Pd-Si distribution has changed, and thus the silicon segregation at low coordinated sites is enhanced.

The physisorption of helium atoms on the amorphous surface showed that physisorption does not have any significant effect on the surface structure or composition. Reconstruction and surface segregation were not induced by physisorption. The physisorption can only slightly reduce the contraction of the surface. This can be understood in the light of the nature of physisorption,

since only a physical interaction exists between the surface of the glass and the helium atoms, a much smaller cohesive energy than Pd-Pd and Pd-Si.

The model of the Pd-Si glassy surface predicts very significant shifts in C.N. For example, the difference between C.N. for the two unrelaxed boundary conditions (4.86 and 6.25) is about 1.4. The difference between C.N. for a (111) close packed plane and a 10A particle, Figure 12, (9.00 and 6.85) is 2.2. The shift in catalytic selectivity as the surface roughness of a noble metal surface structure changes from a close packed plane to a small particle is dramatic [19], and is the basis for the concept of structure sensitivity in catalyzed reaction [20]. The shifts of C.N. upon relaxation of the two extremes in unrelaxed glasses are 0.78 in the rough surface case (4.86 ---> 5.64) and 0.30 in the smooth surface case (6.24 ---> 5.94). Both of these C.N. shifts are greater than the shift going from a (111) close packed plane to a very rough, stepped and terraced (10 8 7) plane, 0.25 (9.00 ---> 8.75). Again, strong differences in catalytic selectivity over such planes have been observed by Somorjai and workers [21].

The calculated fractal dimension of the glassy surface of 2.3 implies a surface roughness on the atomic scale, as shown in Figure 7. This scale of roughness was observed by Huntley et al [22] by Low Energy Ion Scattering measurements on $\text{Fe}_{80}\text{B}_{20}$ metallic glass.

e. Conclusions

The amorphous surface simulated in this paper is rough on an atomic scale with an coordination number ranging from 4-11. This

surface coordination number can be compared to high Miller index planes ranging from 6-11 and small particles ranging from 6-9. The roughness of the metallic glass surface is described in terms of distribution functions of the surface coordination numbers and by a fractal surface dimension of 2.3. The average surface coordination number of the glass is lower than that for a small particle and much lower than that of a nominally flat crystallographic plane.

f. References

1. D. E. Polk, Scripta Met. 4 (1970) 117.
2. C. H. Bennett, J. Appl. Physics 43 (1973) 2723.
3. J. A. Barker, Nature 257 (1970) 120.
4. B. B. Mandelbrodt, Fractals: Form, Chance, Dimension, San Francisco, W. G. Freeman, (1977).
5. T. M. Hayes, J. Allen, I. Tauc, B. C. Giesen, J. J. Hausen, Phys. Rev. Let. 40 (1978).
6. P. H. Gaskell, J. of Non-Crystalline Solids 37 (1976) 206.
7. S. H. Garofalini, J. of Non-Crystalline Solids 37 (1980) 411.
8. D. S. Boudreaux, T. Halicioglu, G. M. Pound, J. Appl. Physics 48 (1977) 5066.
9. M. G. Duffy, J. of Non-Crystalline Solids 27 (1976) 206.
10. V. Vatolin, Y. Kozlow, E. Pastukhov, SIAN Metallurgy 5 (1977) 181.
11. G. S. Cargill III, M. A. Hoare, J. L. Finney, Solid State Physics ed. D. Turnbull 30 (1975) 227.
12. G. A. Somorjai, Chemistry in Two Dimensions: Surfaces, Cornell University Press, Ithaca, 1981.
13. P. W. Davies, Surface Science 110 (1981) 227.
14. M. G. Gillet, R. M. Lambert, Surface Science 90 (1978) 91.
15. P. Gallezot, R. Renou, Nouveau J. de Chimie 2 (1978) 263.
16. M. J. Ledoux, Nouveau J. de Chimie 2 (1979), p. 9.

17. W. E. Brower, G. V. Smith, T. L. Pettit, M. S. Matyjaszczyk, Nature 301 (1983) 47.
18. D. W. Blakely and G. A. Somorjai, Sur. Sci. 65 (1977) 419.
19. D. J. Dwyer and G. A. Somorjai, J. Catal. 56 (1979) 249.
20. M. Boudart, Adv. Catal. 27, 153 (1969).
21. S. M. Davis and G. A. Somorjai, J. Catal. 65 (1980) 78.
22. D. R. Huntley, S. H. Overbury, D. M. Zehner, J. B. Budai, and W. E. Brower, Jr., Applied Surf. Sci. 27 (1986) 180.

2. HVEM at Argonne National Laboratory

Amorphous Pd₈₀Si₂₀ flakes produced by the shock tube technique have been used as catalysts in hydrogenation and isomerization reactions of olefins [1,2]. Amorphous Pd₈₀Si₂₀ exhibits altered selectivity with respect to a crystalline Pd catalyst [2] and amorphous Fe₈₀B₂₀ [3]. the Fischer-Tropsch reaction requires a temperature of 300-400°C, which is in the range of crystallization temperatures for Fe₈₀B₂₀ glass in inert atmosphere and vacuum. Thus, knowledge of the kinetics of crystallization both in inert and reactive atmospheres is essential, if such non-equilibrium catalysts are to be maintained as glasses in hydrocarbon reactions.

It was reported by Masumoto et al. [3] that the crystallization temperature of Fe₈₀B₂₀ amorphous ribbon was lowered by 132° C during the Fischer-Tropsch reaction. They also observed up to a hundred times lower reaction rate after crystallization. It was found by E. E. Alp et al. [4] that the crystallization of Fe₈₀B₂₀ glass in the presence of inert gas differs from the crystallization in vacuum. Wagner et al. [5] found a difference in the crystallization kinetics as a function

of annealing atmosphere for $\text{Fe}_{78}\text{Mo}_2\text{B}_{20}$ metallic glass alloy. The crystallization temperature was higher in one atmosphere of argon as compared to 10^{-7} torr vacuum.

Here we report the study of the crystallization of $\text{Pd}_{80}\text{Si}_{20}$ alloy glass in vacuum and in a cyclohexane atmosphere by using the High Voltage Electron Microscope (HVEM) in conjunction with an in situ environmental cell available at Argonne National Laboratory.

a. Experimental Procedure

The samples were prepared by using "shock tube" rapid solidification technique [6] from a master alloy of the composition $\text{Pd}_{80}\text{Si}_{20}$. The use of the HVEM at Argonne National Laboratory, which is equipped with 1.2 MeV accelerating voltage, enables the study of unthinned flakes produced by out shock tube splat cooler due to the useful depth of penetration of the electron beam of $1\ \mu\text{m}$. The resolution of the HVEM in the imaging mode is 3 angstroms. Using unthinned samples prevented spurious crystallization effects due to the electrolytic thinning process [7] and allows an evaluation of adsorption effects on the glassy surface which would be inserted into a reactor. The shock tube produced flakes are nominally 5 microns thick, but have an irregular thickness with occasional holes. Large areas of the unthinned flakes are thin enough to become electron transparent at the high electron energies available in the HVEM. Two samples of $\text{Pd}_{80}\text{Si}_{20}$ were studied, one in normal TEM column vacuum of 10^{-6} torr, and the second in the presence of 20 torr cyclohexane. The first sample in the vacuum was heated in a stepwise procedure by successive 20 minute isothermal treatments at 150°C , 300°C ,

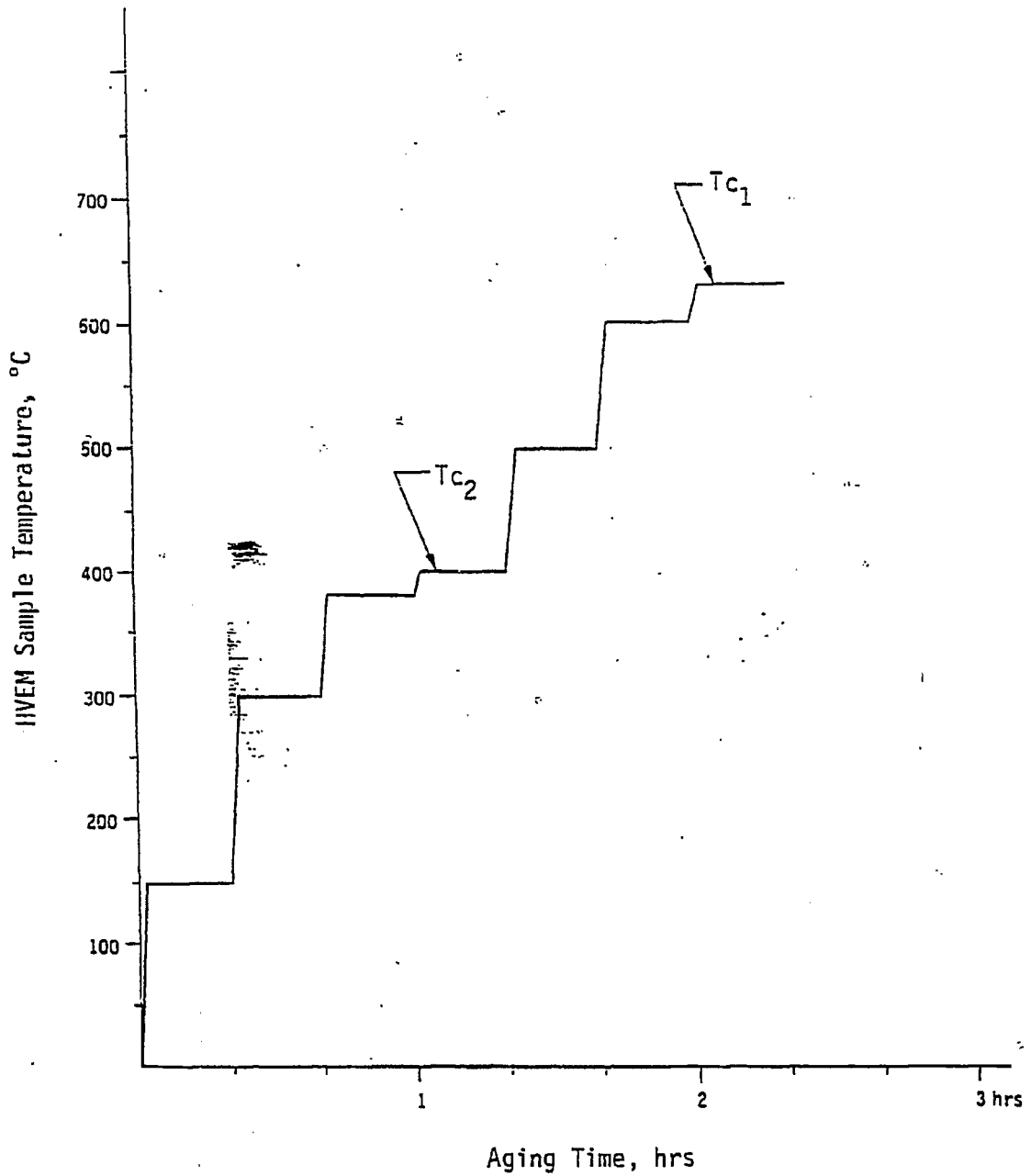


Figure 13. Stepwise aging procedure utilizing HVEM hot stage. Onset of crystallization in vacuum, T_{c1} ; onset of crystallization in cyclohexane, T_{c2} .

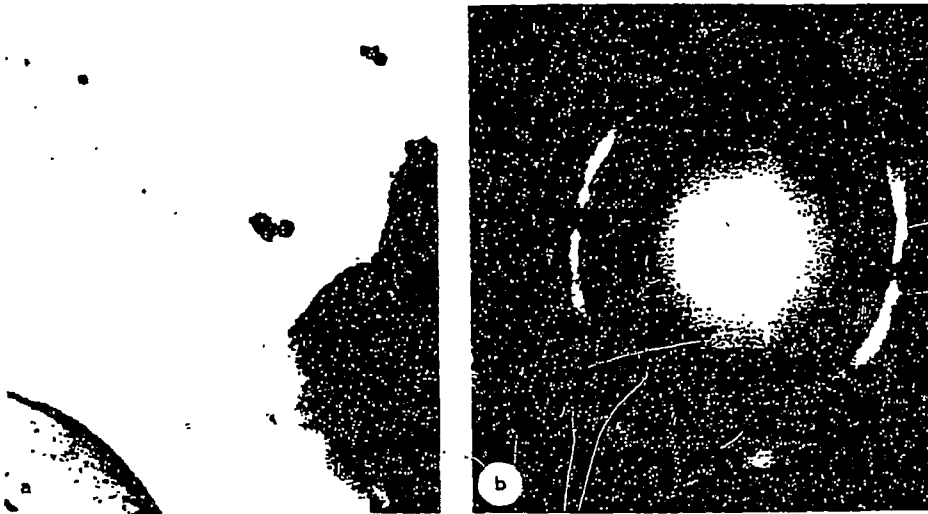


FIG. 14 (a) Transmission electron micrograph of $\text{Pd}_{40}\text{Si}_{20}$ unthinned sample as quenched, showing small crystallites immersed in an amorphous matrix, $24,000\times$. (b) Diffraction pattern of $\text{Pd}_{40}\text{Si}_{20}$ sample in (a). The glassy band is very faint.

400°C, 500°C, 600°C, and 630°C, shown schematically in Figure 1. Heating to the next higher holding temperature took 1-2 minutes. The second sample was heated by the same procedure up to 450°C. The difference between the two actual temperatures, 400°C and 405°C (both nominally 400°C), arose from differences in resetting the hot stage power supply.

b. Results

i) Vacuum Aging

The diffraction pattern and the image of the unaged Pd₈₀Si₂₀ sample in vacuum at room temperature are shown in Figure 14. A low density of small crystallites can usually be detected in some sections of the as quenched sample by imaging, but not by diffraction. The diffraction pattern showed only two diffuse bands indicating an initially glassy structure. The apertures used in the HVEM Environmental Cell prevent viewing diffraction at higher scattering angles. The same diffraction pattern and image were obtained at each isothermal vacuum aging step up to 600°C. At 630°C the diffraction lines attributed to Pd₉Si₂ and Pd₃Si appeared in place of the glassy bands. The emerging diffraction pattern of Pd₈₀Si₂₀ sample at 630°C is shown in Figure 3b. The corresponding image shown in Figure 3a shows a dense population of 500 Å crystallites. The measured d spacings and estimated relative intensities of the observed diffraction lines are shown in Table 2. Shown for comparison in Table 2 are the results of the Duhai et al. [9] and Masumoto and Maddin [10] for vacuum aging of Pd₈₀Si₂₀.

Two of these lines match (221) and (404) lines of Pd₉Si₂, according to crystallographic data provided by Nyland [8]. Duhai

[9] also reported (221) and (404) Pd_9Si_2 lines in TEM diffraction studies of crystallized $\text{Pd}_{80}\text{Si}_{20}$. Except for the first line, with corresponding lattice distance 2.80 Å, all other lines have corresponding d-spacings in good agreement with data provided by Masumoto and Maddin [10] for MS II and Pd_3Si . ME II is a metastable phase formed from $\text{Pd}_{80}\text{Si}_{20}$ glass with an unknown crystal structure [10]. However, the comparison of intensities for our two strongest observed lines in vacuum, 2.50 Å and 2.10 Å, gives a good agreement only with Masumoto and Maddin's data for Pd_3Si .

Three other lines, 1.63, 1.43, and 1.36 Å cannot be compared with the Masumoto data for Pd_3Si , because in that work the smallest lattice distance is 1.800 Å. Line 1.63 Å can be only attributed to MS II. The intensity comparison also gives a good agreement.

Lines 1.43 and 1.36 Å are also in good agreement with MS II lines in terms of both lattice distance and relative intensity. They can also match Pd_9Si_2 (404) and Pd_9Si (004) from Duhai's work.

ii) Cyclohexane Aging

The same heating procedure shown in Figure 13 was repeated with another unthinned $\text{Pd}_{80}\text{Si}_{20}$ flake in the presence of 20 torr of cyclohexane in the HVEM environmental cell. The room temperature diffraction pattern of this second sample was identical to the pattern shown in Figure 14b for the vacuum aged sample of $\text{Pd}_{80}\text{Si}_{20}$. During aging at 150°C the image darkened, apparently due to the adsorption of cyclohexane on the metallic glass surface. Below 405°C no crystalline diffraction lines

Table 2. Analyzed results of electron diffraction patterns obtained by stepwise heating of $\text{Pd}_{90}\text{Si}_{10}$ glass in situ in vacuum and cyclohexane. Shown for comparison are the results of Duhalet al (4) and Masumoto and Maddin (11).

Number of Line	HVEM Results				Duhalet*			Masumoto and Maddin			
	vacuum		cyclohexane		Phase (hkl)	$d_L, \text{\AA}$	I obs	Phase (hkl)	$d_L, \text{\AA}$	I obs	
	Lattice Distance $d_L, \text{\AA}$	Intensity I obs	Lattice Distance $d_L, \text{\AA}$	Intensity I obs							
1	2.80	M	---	---	$\text{Pd}_9\text{Si}_2(221)$	2.78	---	---	---	---	
2	---	---	2.73	M	---	---	MS11	2.698	W	$\text{Pd}_3\text{Si}(121)$ 2.701 M	
3	2.50	S	2.50	VS	$\text{Pd}_3\text{Si}(012)$	2.40	---	MS11	2.516	W	$\text{Pd}_3\text{Si}(201)$ 2.510 M
4	---	---	2.27	S	---	---	---	MS11	2.270	S	$\text{Pd}_3\text{Si}(031)$ 2.270 S
5	2.10	VS	---	---	---	---	---	MS11	2.098	M	$\text{Pd}_3\text{Si}(221)$ 2.098 S
6	---	---	2.04	VH	---	---	---	MS11	2.017	W	$\text{Pd}_3\text{Si}(122)$ 2.014 M
7	---	---	1.82	W	---	---	---	MS11	1.800	W	$\text{Pd}_3\text{Si}(301)$ 1.800 W
8	1.63	VH	1.64	W	---	---	---	MS11	1.630	VH	---
9	---	---	1.56	W	---	---	---	MS11	1.527	VH	---
10	---	---	1.49	W	---	---	---	MS11	1.483	VH	---
11	1.43	W	1.42	W	$\text{Pd}_9\text{Si}_2(404)$	1.43	---	MS11	1.452	VH	---
12	1.36	H	1.36	H	$\text{Pd}_3\text{Si}(004)$	1.31	---	MS11	1.375	H	---
13	---	---	1.25	VH	---	---	---	MS11	1.244	VH	---

*Corresponding lattice distances calculated from crystallographic data of Nyland (8) for orthorhombic Pd_9Si_2 : $a = 7.418 \text{\AA}$, $b = 9.396 \text{\AA}$, $c = 9.048 \text{\AA}$, and from Nyland and Aronson (12) for orthorhombic Pd_3Si : $a = 4.735 \text{\AA}$, $b = 7.555 \text{\AA}$, $c = 5.260 \text{\AA}$

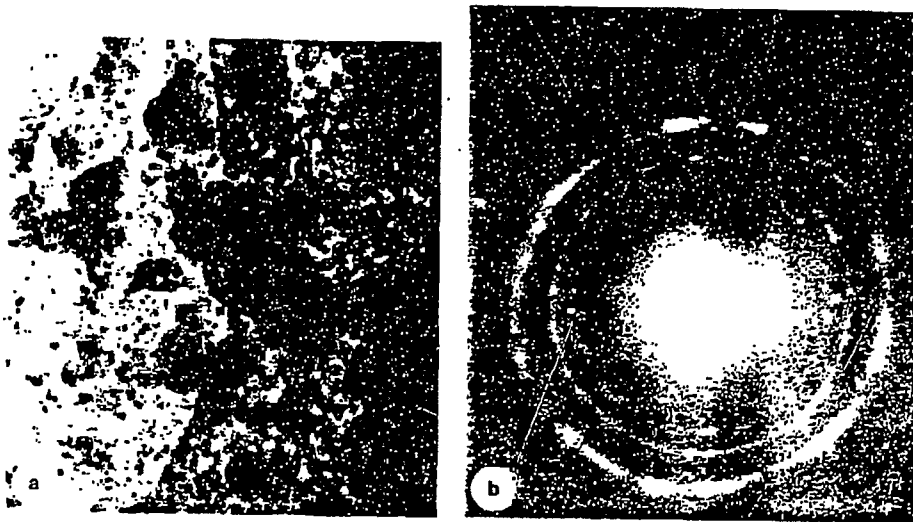


FIG 15 (a) Transmission electron micrograph of $\text{Pd}_{40}\text{Si}_{20}$ sample heated to 630°C in vacuum, showing a dense population of $500\text{-}\text{\AA}$ crystallites, $240,000\times$. (b) The diffraction pattern of $\text{Pd}_{40}\text{Si}_{20}$ sample from (a).

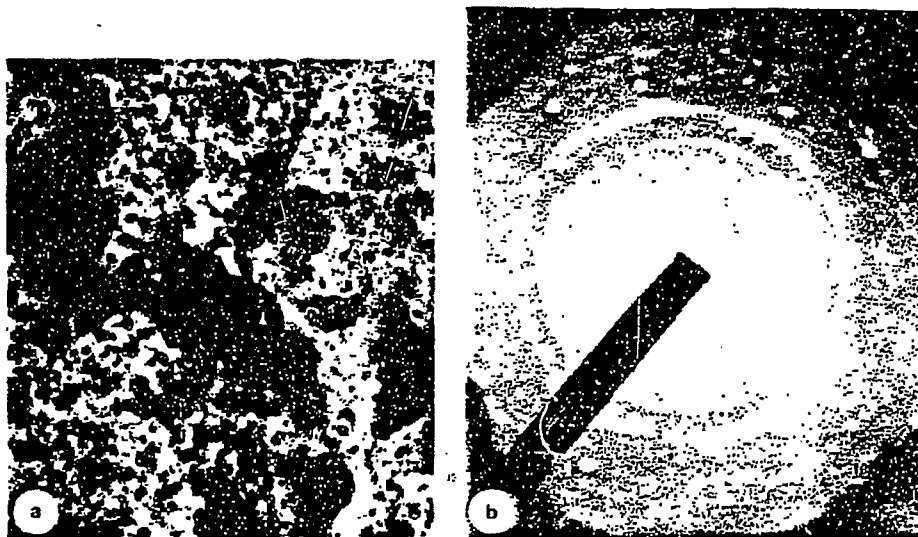


FIG 16 (a) Transmission electron micrograph of the unthinned $\text{Pd}_{40}\text{Si}_{20}$ sample heated to 405°C in the presence of cyclohexane, showing a dense population of $1000\text{-}\text{\AA}$ crystallites, $24,000\times$. (b) Diffraction pattern of the $\text{Pd}_{40}\text{Si}_{20}$ sample from (a).

emerged. At 405°C diffraction lines emerged as shown in Figure 16b; the image showed a dense population of 1000 Å crystallites, Figure 16a.

The measured d-spacings and estimated relative intensities of the observed diffraction lines from cyclohexane aging are also shown in Table 2 for comparison to the vacuum aging results. The relative intensities of the two strongest lines, 2.40 Å and 2.27 Å, are in good agreement only with Pd₃Si [10]. The measured d-spacings for the first five lines match both Pd₃Si and MS II [10]. In the presence of cyclohexane seven new lines appeared, all of which are in the d-spacing range for measured diffraction lines in the vacuum aged sample. Two lines at 2.80 Å and 2.10 Å which appeared at medium and very strong intensities during vacuum aging, did not appear during aging in cyclohexane. Three of the new lines are in good agreement with data for Pd₃Si [10] in terms of both d-spacings and relative intensity. Four of them are in good agreement with MS II [10] in terms of both relative intensity and d-spacings.

c. Discussion

The environmental cell and the hot stage of the HVEM made possible the study of the crystallization of Pd₈₀Si₂₀ glass in situ both in vacuum and in conditions simulating a reaction. The crystallization temperature was found to be 630°C in vacuum. The transformation of Pd₈₀Si₂₀ to Pd₃Si was reported before in vacuum at 500°C [9]. The presence of cyclohexane had a significant effect on the crystallization of Pd₈₀Si₂₀ glass sample. The crystallization temperature was lowered by about 200°C, Figure 1. This kind of adsorption effect on the bulk crystallization of a

metallic glass was reported before Masumoto et al. [3], who reported a 132°C lowering of the crystallization temperature of Fe₈₀B₂₀ glass during the Fischer-Tropsch reaction.

The other effect of cyclohexane adsorption was to alter the path of the phase transformation of the Pd₈₀Si₂₀ metallic glass itself. As can be seen in Table 2, four diffraction lines are common to both aging atmospheres. Three out of these four lines index well to Pd₃Si. Two of the lines in the vacuum aging pattern do not appear in the cyclohexane pattern 2.10 Å, associated with Pd₃Si, and 2.80 Å associated with Pd₉Si₂. Thus, it appears that the Pd₃Si phase is common to both atmospheres, but the Pd₉Si₂ does not appear in cyclohexane. Since all seven new lines in the cyclohexane pattern can be associated with MS II and Pd₃Si, the cyclohexane aging atmosphere apparently induces the crystallization of a MS II second phase with Pd₃Si, whereas the vacuum aging induces a Pd₃Si and Pd₉Si₂ two phase structure. Although the above interpretation of the crystal structures appearing on aging is not without ambiguity, the strong differences between the two diffraction patterns clearly indicate a different crystallization path for Pd₈₀Si₂₀ glass in vacuum as opposed to cyclohexane.

The change of the crystallization path for Pd₈₀Si₂₀ glass in the presence of cyclohexane differs from the effect of adsorbed reactants observed by Masumoto et al., where the reaction conditions lowered the crystallization temperature of Fe₈₀B₂₀ glass, but did not effect the structure of the transformed glass.

The darkening of the TEM image after exposure to cyclohexane indicates at least physisorption and probably chemisorption of

the cyclohexane occurred. Such chemisorption induced glass crystallization could be the analog of chemisorption induced surface segregation as observed by Sachtler and coworkers [11].

The authors feel that the enhancement of crystallization kinetics by the presence of chemisorbed cyclohexane may be evidence for a sort of catalysis in reverse. Just as the reactant molecules are faced with an activation energy barrier, the metastable glassy structure, which comprises the $\text{Pd}_{80}\text{-Si}_{20}$ alloy catalyst, is attempting to crystallize by surmounting the activation barrier for crystallization. The usual case for the rate limiting step in phase transformations of alloys in the solid state is diffusion of solute. Thus, it appears that the chemisorbed cyclohexane weakens the bonds between surface palladium and silicon atoms and allows surface diffusion and the subsequent crystallization at a higher rate than the vacuum case.

d. Conclusions

The adsorption of cyclohexane has a strong effect on the crystallization kinetics of the metastable $\text{Pd}_{80}\text{Si}_{20}$ metallic glass. The crystallization temperature was lowered by 200°C as compared to vacuum conditions. In addition, the path of the crystallization was altered from vacuum conditions, which apparently generate a mixture of Pd_3Si and Pd_9Si_2 , to cyclohexane conditions, which generate a mixture of Pd_3Si and MS II.

e. References

1. Smith, G. V., Zahraa, O., Molnar, A., Khan, M. M., Richter, B., Brower, W. E., J. Cat. 83, 238 (1983).
2. Brower, W. E., Jr., Matyjaszczyk, M. S. Pettit, T. L., and Smith, G. V., Nature 301, 497 (1983).
3. Yokoyama, A., Komiyama, H. Inoue, H. Masumoto, T., and

- Kimura, H. M., J. Cat. 68, 355 (1981).
4. Alp, E. E., M. Saporoschenko, and Brower, W. E., Jr., in "Proceedings of the Conference of Rapidly Quenched Metals", Wurtzburg, West Germany, 1984.
 5. Wagner, C. J., Advan. X-ray Anal. 12, 50 (1969).
 6. Duwez, P., Trans. ASM 60, 605 (1967).
 7. Scott, M. G., "Crystallization" in Amorphous Metallic Alloys, F. E. Loborsky, ed., Butterworths, London, 1983.
 8. Nylund, Anna, Acta Chem. Scan., 20, 2381 (1966).
 9. Duhaj, P., Sladek, V., and Mrafko, P., J. Non-Crystalline Solids 13, 341 (1973).
 10. Masumoto, T. and Maddin, R., Acta Met., 19, 725 (1971).
 11. Bouwman, R., Lippits, G. H. M., and Sachtler, W. M. H., J. Catal. 25, 350 (1972).
 12. Aronsson, B., Acta Chem. Scand., 20, 2381 (1966).

3. Ion Scattering Spectroscopy - Oak Ridge National Laboratory (with S. Overbury and D. Huntley)

Amorphous materials such as metallic glasses do not have long range order and as such their structure is not describeable by a repeating unit cell as for crystalline materials. They do, however, exhibit short range order, as observed by x-ray diffraction studies, indicating that the local environment is similar from atom to atom. There is also evidence that there are "associations" of atoms in some met-glasses as well as a certain concentration of microcrystallites. It is interesting to consider the following questions.

How is the bulk structure terminated at the surface?

Is the surface "rough" on an atomic scale, or is it smooth due to minimization of surface free energy?

Are there facets corresponding to the boundaries of associations?

Does crystallization begin at the surface?

Is the composition of the surface the same as the bulk?

Are there differences between the rapidly cooled side and the free surface side of the quenched ribbon or splat?

Although virtually nothing is known about such surfaces, catalytic studies on $\text{Pd}_{80}\text{Si}_{20}$ glasses have indicated that the surface is very "rough" as indicated by selectivity differences between amorphous and crystalline surfaces. We have applied low energy ion scattering to study the surface of $\text{Fe}_{80}\text{B}_{20}$ glass (Allied Chemical, Metglass 2605) in an attempt to measure and ultimately define and quantify this roughness. Ion scattering is an ideal tool since it is structure sensitive and probes local ordering. One way in which surface roughness affects ion scattering is in the incident angle dependence. Consider an experiment in which the intensity of scattered ions is measured at a fixed scattering angle (60°) as a function of the angle of incidence. At very grazing angles of incidence ($\psi < 10^\circ$), scattering from any atom in a single crystal surface is not possible due to shadowing by its neighbors. Similarly, grazing exit angles ($\psi > 50^\circ$) are blocked by nearest neighbors. On an amorphous surface scattering may occur from atoms which protrude above the surface and are unshadowed by neighbors. It is therefore expected that for a single crystal the intensity will drop off the very low values at small and large incidence angles, while scattering from an amorphous surface is expected to be relatively more intense at these extremes. Averaging over many configurations of atoms should also broaden and smooth out the angular distributions. These ideas can be tested on a single crystal. In the Figure 17 the dependence of the single

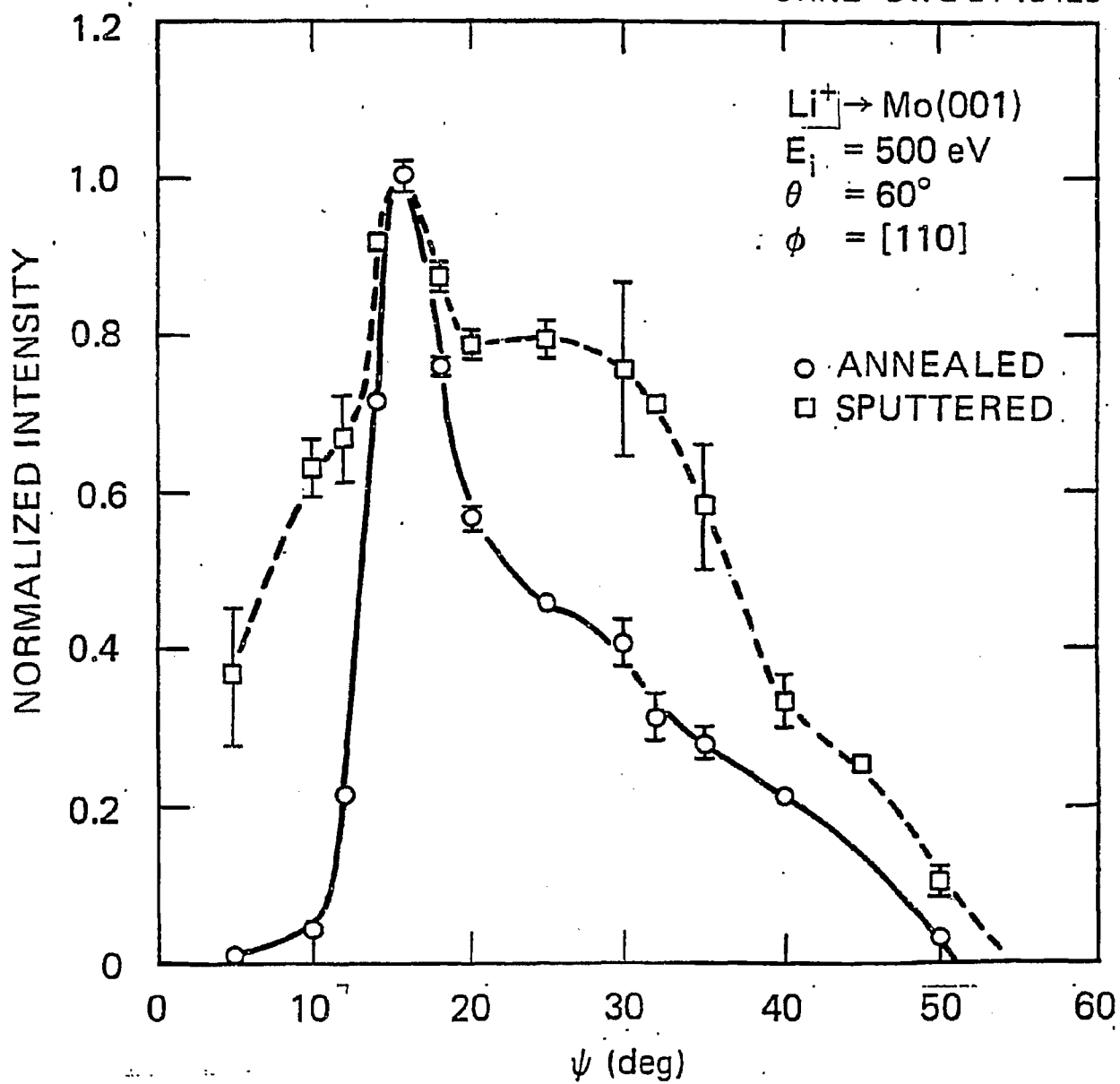


Figure 17. LEIS of Mo (001)

scattering peak height for Li^+ scattering from $\text{Mo}(001)$ is shown as a function of incident angle. The annealed surface gives a distribution characteristic of all single crystal surfaces, which shows a sharply peaked maximum and an abrupt cut-off at more grazing incidence angles. The distribution shows also a drop in intensity at low exit angles (large incidence angles). If the surface is roughened, for example by sputtering, the distribution is broadened considerably although a remnant of undamaged surface remains. The dependence upon incident angle was measured for an amorphous $\text{Fe}_{80}\text{B}_{20}$ foil. The angular distribution is very broad as shown in the Figure 18, and exhibits a relatively high intensity at small and large incidence angles as expected for a rough surface. The surface was cleaned by sputtering, removing most but not all impurities and was gradually crystallized by a sequence of annealing steps. The angular dependence was measured repeatedly as a function of these treatments. Annealing briefly to 300°C , was sufficient to cause changes in the Fe/B concentration ratio (according to ~~AES~~), but did not change the shape of the angular distribution. Only very minor changes are observed after extensive annealing at 400°C or finally to 600°C , sufficient to crystallize the bulk. Both sides of the amorphous ribbon were examined. The "bottom" side is the side closest to the cooling substrate when the net-glass is quenched from the melt. There have been contradictory reports as to whether the free "top" side of the ribbon which cools slower than the bottom side, is partially crystallized in the as-quenched state. The angular distribution for the top surface is shown in Figure 19. The distribution changed slightly with increasing sputter dose,

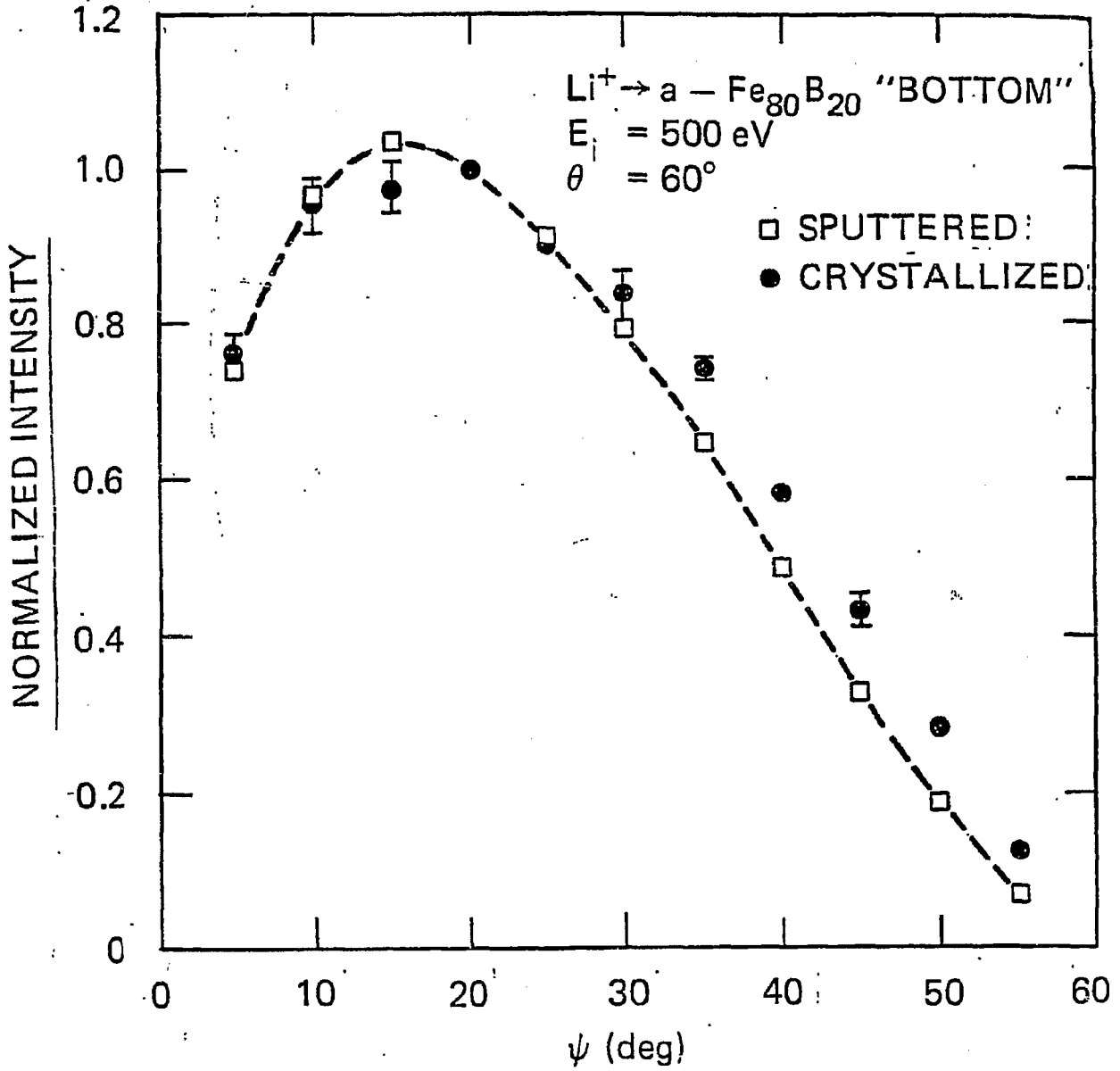


Figure 18. LEIS of Fe₈₀B₂₀ Bottom

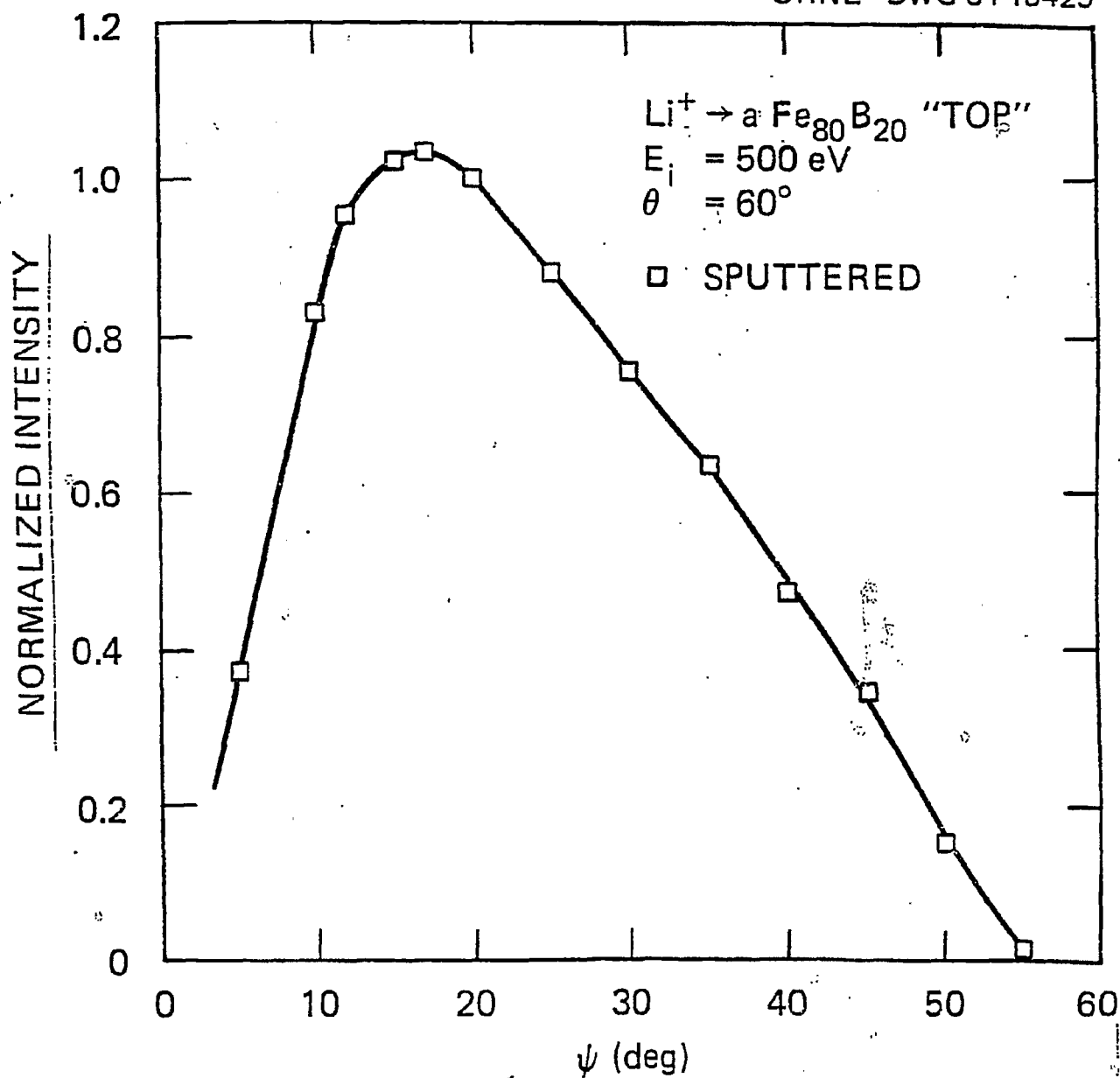
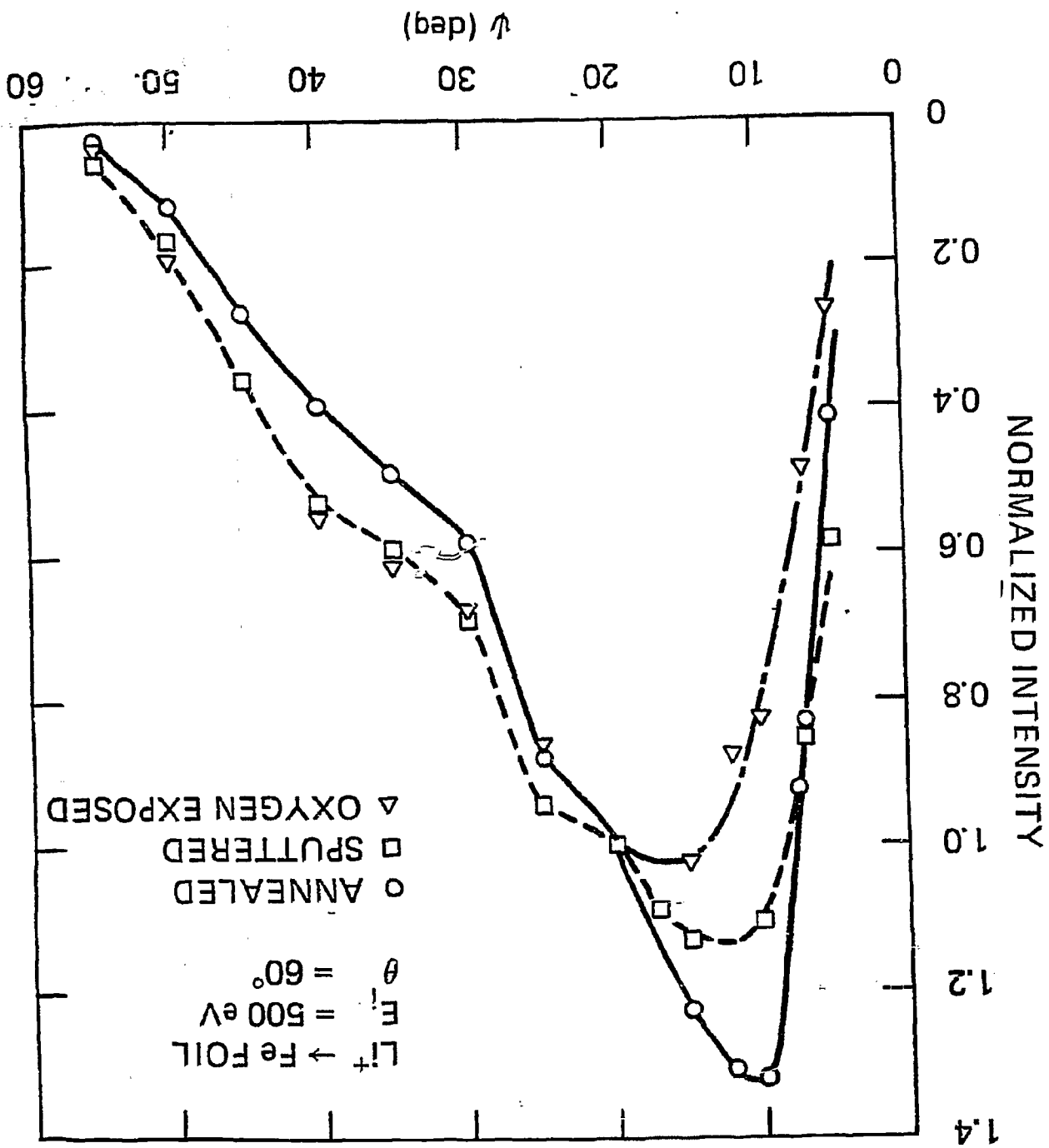


Figure 19. LEIS of Fe₈₀B₂₀ Top

exhibiting a slight increase in relative intensity at low with increasing dose. The distribution obtained after the largest sputter dose is shown. No annealing was done on this sample. The distribution is relatively less intense at low and high compared to the bottom side consistent with a higher crystallization fraction.

To interpret the angular distributions, it is necessary to know more about the effects of surface impurities and macroscopic roughness (undulations, scratches, etc.). It is also interesting to consider whether an average of the many crystallite grains in various orientations present in a polycrystalline material would give rise to such a broadened angular distribution. In an attempt to answer this last question, a polished polycrystalline Fe foil was examined and the resulting angular distribution is shown in Figure 20. This sample exhibited a cut-off which was sharper than that for the amorphous samples. However, changes in the angular distribution were observed when the ion beam was moved to other points on the surface. Thus the desired goal of averaging over many grains was not achieved. The effect of surface impurities was determined by exposure of the polycrystalline Fe to oxygen. The impurity resulted in a shift in the maximum to higher but a fairly sharp cut-off, and low relative intensity at low and high remained.

The angular distributions are expected to be affected by microscopic roughness which could cause large-scale shadowing and blocking at low incident or exit angles. To check for this possibility the cross sections of representative $\text{Fe}_{80}\text{B}_{20}$ ribbon were examined by SEM. Undulations on the bottom side of up to



ORNL-DWG 84-13428

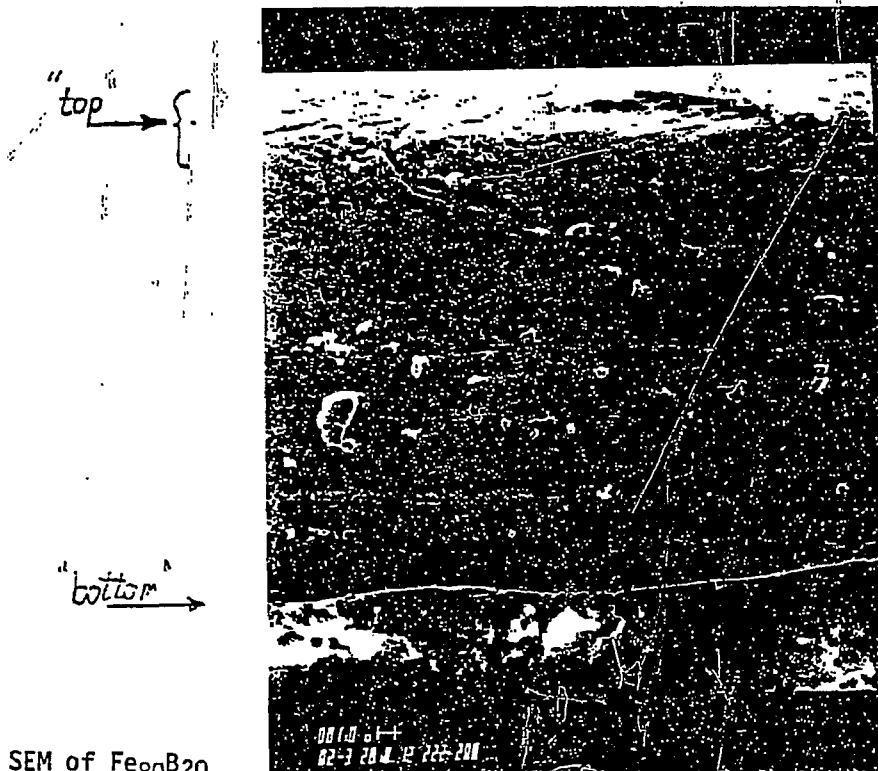
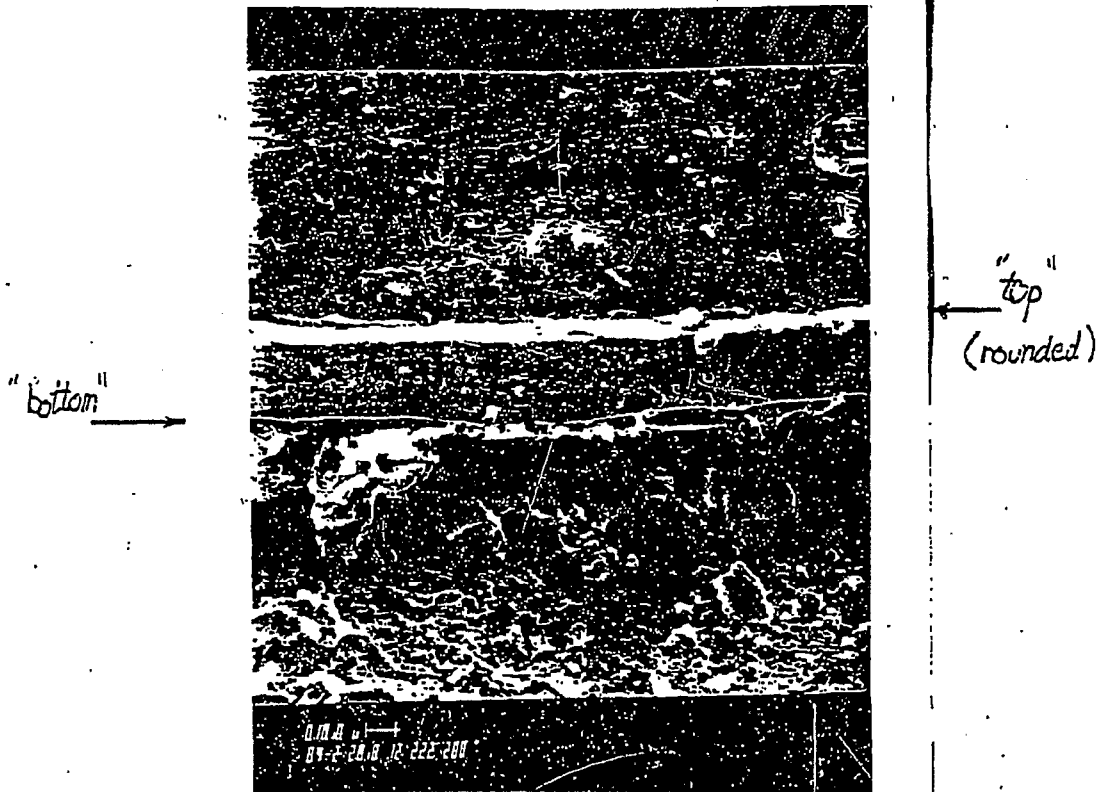


Figure 21. SEM of Fe_{0.8}B_{2.0}

6° from the macroscopic surface plane were observed Figure 21, while the top side was considerably smoother. Such undulations could be partly responsible for the observed differences in the angular distributions of the top compared to the bottom side of the ribbon.

Differences in composition were also observed between the two sides as determined from measuring the B/Fe Auger intensity ratio as a function of various treatments of the samples. The results are summarized above. Both surfaces exhibited an increase in B/Fe ratio with sputtering while the bottom side showed relative enrichment in B compared to the top surface. This enrichment decreased with annealing. It has been proposed that during the crystallization of Fe₈₀B₂₀, α-Fe crystallizes on the surface resulting in the loss of B from the surface. These results from extensive annealing experiments are consistent with this proposal.

a. Conclusions

1. >The angular dependence of the ion scattering intensity shows sensitivity to roughness on an atomic scale.
2. >The ion scattering data for the Fe₈₀B₂₀ foil indicates that the surface is rough at an atomic level and that this roughness is only slightly affected by bulk crystallization.
3. >The surface becomes depleted of boron with crystallization, suggesting a phase distribution where the surface is enriched with alpha iron.
4. >There are differences between the 'top' and 'bottom' sides of the foil. >Both the ion scattering and Auger data suggest that the 'top' side is somewhat more crystalline than the 'bottom' side.

4. Conversion Electron Moessbauer Spectroscopy

Conversion Electron Moessbauer Spectroscopy, CEMS, along with conventional transmission Moessbauer spectroscopy is used to

determine near surface crystallization behavior of $\text{Fe}_{80}\text{B}_{20}$ (MG 2605) metallic glass. Single roller quenched samples were heat treated isothermally under inert atmosphere and in vacuum. The relative amounts of residual amorphous phase and crystallization products are determined. As predicted by Newtonian splat cooling conditions, no preferred crystallization is observed at the top or bottom of the sample as compared to the bulk during the course of the isothermal crystallization. The predominant crystalline product in the as quenched glass Fe_3B , indicating such short range ordering in the glassy state. However, upon isothermal aging, substantial amounts of γ -Fe crystallize both near surface and in the bulk.

a. Introduction

The crystallization of $\text{Fe}_{80}\text{B}_{20}$ metallic glass is probably one of the most extensively studied phase transformation in recent years. The superior mechanical and magnetic properties of Fe-B based metallic glasses make them technologically very attractive. However, it is also known that upon initiation of crystallization they become very brittle, and high permeability and the low coercive force are lost. On the other hand, crystallization of $\text{Pd}_{41}\text{Si}_{59}$ glass does not substantially diminish the unusually selective behavior in hydrogenation reaction. Similarly, the corrosion resistance of Fe-Ni-Cr-W alloys upon partial crystallization is initially maintained. However, later, due to a redistribution of major metallic components between amorphous and crystalline phases, corrosion resistance degrades. Therefore, it is important to compare surface and bulk crystallization kinetics in metallic glasses. In this work ^{57}Fe

transmission Moessbauer spectroscopy has been used simultaneously with CEMS to monitor the relative rates of near surface versus bulk crystallization.

b. Experimental Procedure

Based on our previous Moessbauer spectroscopy and differential scanning calorimetry, DSC, work, $\text{Fe}_{80}\text{B}_{20}$ metallic glass ribbon (obtained from Allied Chemical Co., NJ, USA) was isothermally heat treated under vacuum (5×10^{-5} torr) at 603 and at 638 K, and under helium atmosphere at 663 K. CEMS measurements on both sides of the ribbon were taken using the flow-type back-scattering detector. A He-10% CH_4 gas mixture, flowing at a rate of 70 cc/min was used to detect 7 keV conversion electrons. The escape depth is found to be approximately 2500 Å by CEMS analysis. A 0.21 μm layer of iron is vapor deposited on a 5 μm thick stainless steel control specimen. The thickness of the film is being measured by a crystal monitor. Figure 22(a) shows CEMS of the coated sample and Fig. 22(b) shows the transmission spectrum of the same sample. From the relative intensity of nearly suppressed stainless steel peak, the escape depth is approximated as 0.25 μm. Since the $\text{Fe}_{80}\text{B}_{20}$ metallic glass ribbons are 35 μm thick, the CEMS sampling depth comprises less than 1% of the total sample.

c. Results and Discussion

Figure 23 shows CEMS and transmission Moessbauer spectra were taken of the quenched and heat treated samples. The relative amounts of amorphous and crystalline phases are determined according to a procedure described by LeCaer. This method allows decoupling of amorphous phases from the crystalline

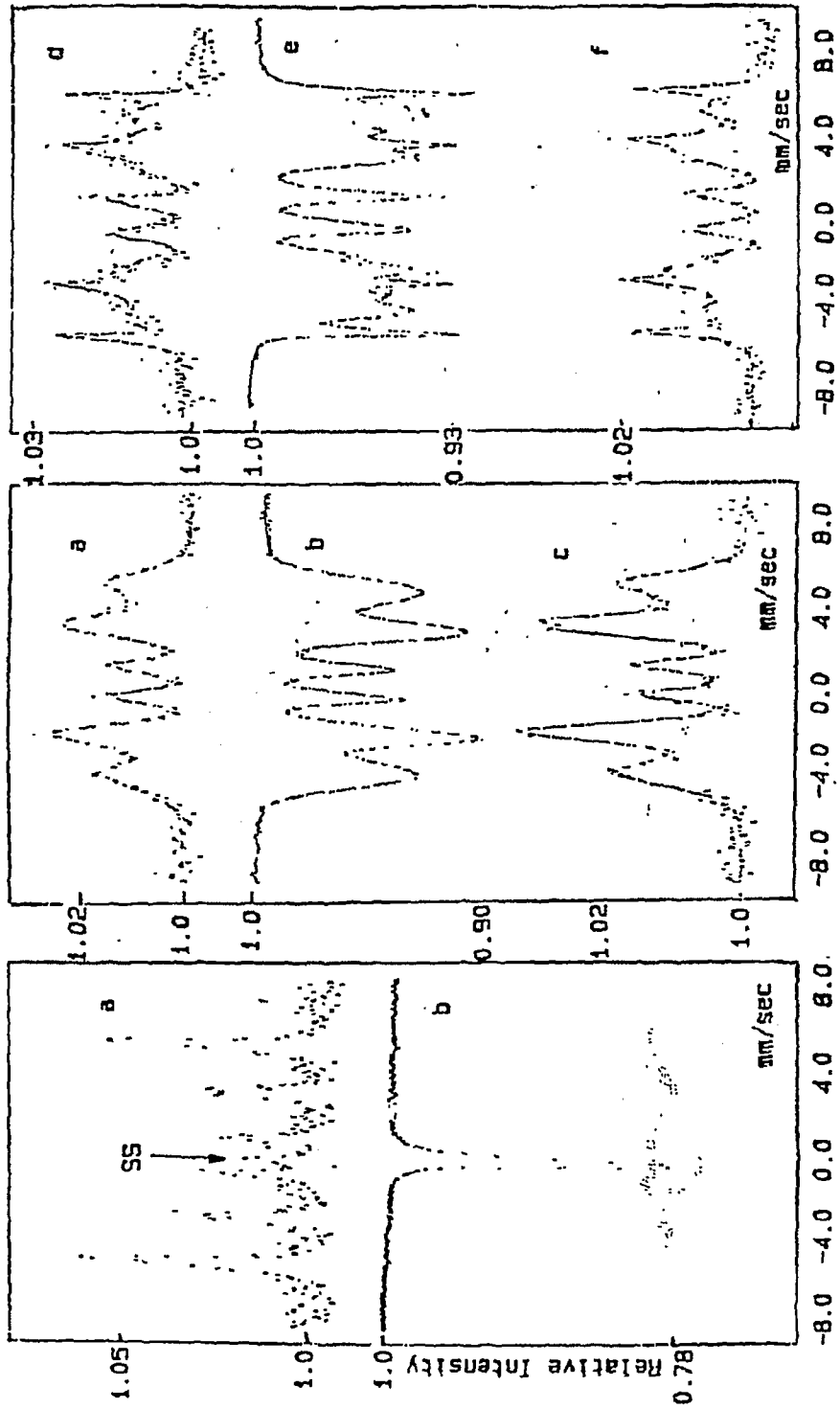


Fig. 22: (a) CEMS of stainless steel with vapor deposited pure iron of 0.21 μ m thickness, (b) transmission spectrum of the same sample.

Fig. 23: Mössbauer spectra of (a) rough side, (b) bulk, (c) shiny side of as quenched Fe₈₀B₂₀ (MG 2605), and (d) rough side, (e) bulk, (f) shiny side of the same sample held at 638 K for 2 hrs. in vacuum.

Table 3. Mössbauer parameters for Fe₃B used in this study (T = 298 K).

Site	H (kOe)	$\frac{eQV_{zz}}{2}$ ($\frac{\text{mm}}{\text{sec}}$)	δ (mm/sec)
1	292	-0.018	0.061
2	280	0.022	0.061
3	268	0.019	0.028
4	255	0.07	0.028
5	266	-0.03	0.105
6	217	-0.03	0.105

Table 4. Average magnetic field of the amorphous phase and the relative distribution of phases in Fe₈₀B₂₀ metallic glass after isothermal heat treatment.

Treatment	Specimen	H (kOe)	57Fe Population			Phase Amounts at %		Composition of the remaining glass, Fe ₈₀ B _x
			in the crystalline phase	in α -Fe	in Fe ₃ B	α -Fe	Fe ₃ B	
as quenched	rough side	253	6	--	6	--	6.4	19.6
	shiny side	253	8	2	6	1.6	6.4	20.0
	bulk	250	5	--	5	--	5.3	19.7
held at 633 K for 30 min. in vacuum	rough side	269	9	--	9	--	9.6	19.3
	shiny side	260	12	3	9	2.4	9.6	20.0
	bulk	251	9	--	9	--	9.6	19.3
held at 638 K for 2 hrs. in vacuum	rough side	252	33	25	8	20	8.5	26.4
	shiny side	277	29	22	7	17.6	7.5	25.5
	bulk	250	35	25	10	20	10.6	26.6
held at 663 K for 15 min. in He atmosphere	rough side	241	5	1	4	0.8	4.3	20.0
	shiny side	247	9	6	3	4.8	3.2	16.7
	bulk	249	4	--	4	--	4.3	19.7
held at 663 K for 30 min. in He atmosphere	rough side	235	8	5	3	4	3.2	16.5
	shiny side	248	9	6	3	4.8	3.2	16.7
	bulk	249	4	--	4	--	4.3	19.7

phases, provided that the line positions and widths of the existing crystalline products are known. The line positions of Fe_3B with bct structure varies somewhat in the literature. Since Fe_3B (t) is a metastable product formed through crystallization from amorphous phase, its crystal and magnetic structure is not well resolved. In this study, we have predicted the line positions by solving the combined electrical quadrupole and magnetic dipole interaction Hamiltonian, by assuming 6 different magnetic lattice positions. The relevant Moessbauer parameters are given in Table 3.

What can be extracted from Moessbauer spectra is actually the relative population of ^{57}Fe in different phases. This relative distribution is then related to the phase amounts in atomic percentages, i.e., number of atoms in the respective phases divided by total number of atoms. Table 4 gives the results for both ^{57}Fe amount in the relevant phases and the phase percentages for different specimens.

An overall view of the results support the expectations of mathematical models of heat and fluid flow during splat cooling. Under Newtonian cooling conditions, no temperature gradients in the splat exist during solidification. Therefore, such splats should be homogeneous through their thickness. Model calculations indicate that Newtonian cooling conditions exist up to a value of Nusselt number of 1.4. For a thickness, $d = 35 \text{ m}$ of $\text{Fe}_{80}\text{B}_{20}$, for interface heat transfer coefficient, $h = 2.0 \text{ cal/cm}^2\text{-sec-k}$, and for a thermal conductivity, $K = 0.12 \text{ cal/cm}^2\text{-sec-K}$, the Nusselt number $N_{\text{Nu}} = h \cdot d / k$ is well within the Newtonian range. By monitoring crystallization

simultaneously with CEMS and transmission Moessbauer spectroscopy, we have determined that, indeed, neither side of the splat is preferred over the bulk for crystallization, within the precision limits of the data which is estimated to be 3%. As can be seen in Table 4, the as quenched $\text{Fe}_{80}\text{B}_{20}$ showed a slightly higher crystallization near the surface region with no substantial preference to either shiny or the rough side. The shiny side of the specimen is in contact with the atmosphere, while the rough side is in contact with the roller during quenching. One should also note that the statistical variation in the CEMS is higher as compared to transmission data due to the lower efficiency of the flow-type detectors. In fact, even in the specimen heat treated at 638 K for 2 hrs. in vacuum, with a substantial crystallization (Fig. 23(b)), neither side or the bulk is preferred for crystallization. The low temperature inert atmosphere heat treatments at 663 K were prepared with the expectation that any initial difference between the surfaces and bulk can be arrested. However, the results indicate otherwise.

c. Conclusions

We have shown that the as quenched $\text{Fe}_{80}\text{B}_{20}$ (MG 2605) metallic glass has a uniform structure through its thickness. Furthermore, it crystallizes uniformly with no appreciable preference on either surface, both in vacuum and under inert atmosphere. The as quenched glass contains some crystallization in the form of Fe_3B .

B. Bulk Analyses

1. Moessbauer Spectroscopy

Moessbauer spectroscopy has been utilized to examine the

bulk structure of the $\text{Fe}_{80}\text{B}_{20}$ metallic glass. Figure 24 shows the spectra and hyperfine field distributions for the as-received $\text{Fe}_{80}\text{B}_{20}$ glass (Allied Chemical Metglas 2605, single roller splat cooler) and the same alloy remelted and quenched at about 10^7 °C/sec. in our shock tube splat cooler. The two Moessbauer spectra are not distinguishably different, and both the hyperfine field distributions indicate a glassy structure. In Figure 25 the spectra of the splats produced in our hammer and anvil splat cooler at lower cooling rates (10^5 - 10^6 °C/sec) show significant crystallization. The Moessbauer spectra of the as-received glass and the fully crystallized glass are compared in Figure 26. The sharp peaks of the crystalline structure correspond to the two equilibrium phases, almost pure bcc α -Fe and the very boron enriched Fe_2B phase.

2. DSC/DTA - 8ICC

The crystallization kinetics for the $\text{Fe}_{80}\text{B}_{20}$ and Zr_2Ni glasses have been determined by a combination of differential scanning calorimetry (DSC) and isothermal vacuum aging. As-received Zr_2Ni glass, (Phillips Corp., Eindhoven, The Netherlands, single roller splat cooler) was found to be slightly crystallized via transmission electron microscopy, whereas the remelted Zr_2Ni alloy which was quenched in our shock tube splat cooler, Figure 27, was completely amorphous (19). Similar to the Zr_2Ni results, Matyjaszczyk observed the as received $\text{Fe}_{80}\text{B}_{20}$ glass (Allied Chemical, single roller splat cooler) to be top surface crystallized via x-ray diffraction (6). Such partial crystallization upon quenching from the liquid may affect the performance of metallic glass catalysts. In addition, the

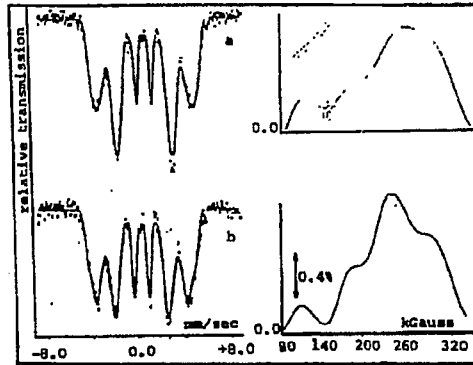


Fig. 24 Moessbauer spectra and the corresponding hyperfine distribution of (a) as-received Mg2605 ribbon, 20 microns thick, (b) $\text{Fe}_{90}\text{B}_{10}$, splat cooled in the shock tube, 2-10 microns thick.

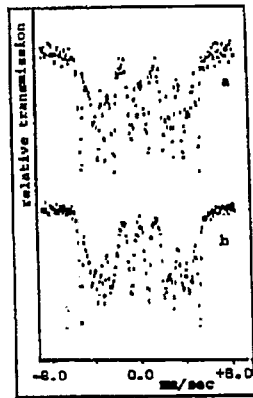


Fig. 25 $\text{Fe}_{90}\text{B}_{10}$ splat cooled in hammer & anvil apparatus with different super heat. Melt temperatures of (a) 1000°C , 33 microns thick and (b) 1350°C , 19 microns thick. In both cases there are appreciable amounts of crystallization which formed during quenching the liquid.

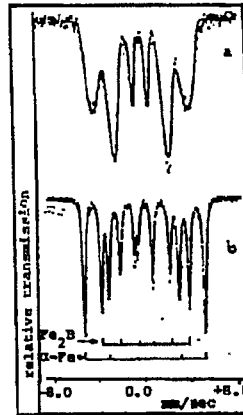


Fig. 26 Moessbauer spectra of (a) as received, amorphous Mg2605 ribbon, and (b) the same sample crystallized at 920°C for 3 hrs. in vacuum. The spectra of the equilibrium phases, α -iron (bcc) and Fe_2B , are labeled.

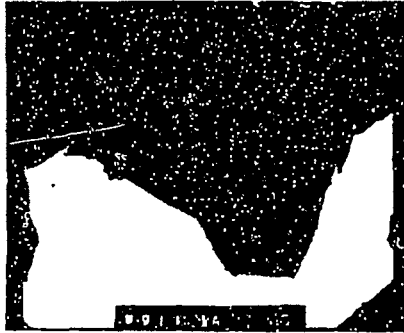


Figure 27 TEM micrograph of a shock tube splatted Zr_2Ni metallic glass. Magnification: 21,000X.

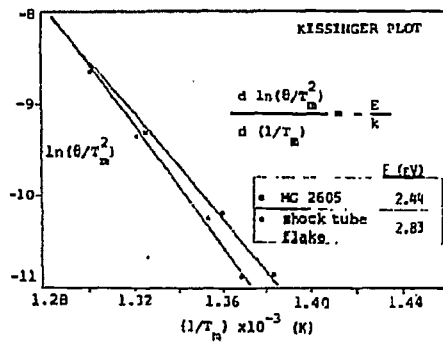


Figure 28 Determination of the activation energy, E, for crystallization of $Fe_{80}B_{20}$ metallic glass based on peak temperature (T_m) shift Kissinger method. -heating rate in the DSC, -as received MG2605 strip, -shock tube flakes from remelted MG2605.

stability of the glassy portion of the splat cooled ribbon is also affected in subsequent thermal treatments (e.g., reaction conditions, isothermal vacuum aging). Figure 28 compares the results of DSC measurements on $\text{Fe}_{80}\text{B}_{20}$ metallic glasses produced by the single roller method and the shock tube method. The pre-existing crystallization in the single roller produced glass apparently has lowered the activation energy for crystallization of the glass phase to 2.44 eV from 2.83 eV in the more completely glassy shock tube produced glass.

3. References

1. Duwez, P., Trans. A. S. M. 60, 605-633 (1967).
2. Brower, W. E., Jr., Matyjaszczyk, M. S., and Pettit, T. L., and Smith, G. V., Nature 301, 497-499 (1983).
3. Smith, G. V., Brower, W. E., Matyjaszczyk, M. S., Pettit, T. L., Proc. 7th Int. Congr. Catalysis (eds. Seiyana, T. and Tanabe, K.,) 355-363 Elsevier, New York 1981.
4. Smith, G. V., Zahraa, O., Khan, M. M., Richter, B., and Brower, W. E., Jr., J. Catal. (in Press).
5. Yokoyama, A., Komiyama, H., Inoue, H., Masumoto, T., and Kimura, H. M., J. Catal. 68, 355-361 (1981).
6. Matyjaszczyk, M. S., Ph. D. Dissertation, Southern Illinois Univ., Carbondale (1981).
7. Greer, A. L., and Leake, J. A. Rapidly Quenched Metals III, Vol. 1, Third Int. Cong., Brighton, 1978.
8. Yosida, S., Yamashita, H., Funabiki, T., and Yonezawa, T., J. Soc. Chem. Common., 964-965 (1982).
9. Yokoyama, A., Komiyama, H., Inoue, H., Masumoto, T., and Kimura, H., Chemistry Letters, The Chemical Society of Japan, 195-198 (1983).
10. Vannice, M. A., Catal. Rev. 14, 153 (1976).
11. Vannice, M. A., J. Catal. 37, 449 (1975).
12. Dwyer, D. J. and Somorjai, G. A., J. Catal. 52, 291 (1978).
13. Aruki, M. and Ponec, V., J. Catal. 44, 439, (1976).

14. Rabo, J. A., Francis, J. N., and Elek, L. F., Proc. Catal. Congr. Tokyo 1980.
15. Alp, E. E., Saporoschenko, M., Simon, K. M., Brower, W. E., Jr., Proc. Congr. Liquid and Amorphous Metals, 1983, in press.
16. Van Meerten, R. Z. C., New Horizons in Catalysis, T. Seiyama and K. Tanabe, editors, Elsevier, New York, 1981.
17. Gaskel, P. H., Nature 276, 484-485 (1978).
18. Kowbel, W. and Brower, W. E., Jr., in preparation.
19. Simon, K. M. and Brower, W. E., Jr., submitted to Metallurgical Transactions A.

C. RSM Processing - Splat Forming Methods

1. Hammer Anvil Discs

Work continues on this method of achieving intermediate cooling rates between the shock tube flakes and the single roller quenched strip. The hammer and anvil, being a two-sided cooling technique, differs from the other two methods in that the most rapidly cooled location is the center of the splat, whereas for the shock tube and single roller, the slowest cooled location is the top surface.

2. Shock Tube Flakes

The shock tube device has been modified by a converging-diverging nozzle design, which causes the droplets to be ejected at supersonic velocities. The former straight bore nozzle design is limited to Mach 1. The flake mean thickness is reduced from 8 microns for the subsonic design to 5 microns for the supersonic design. Higher cooling rates should result from the reduced thickness, and this effect is being investigated by splat cooling alloys for which glass formation has proven more difficult, like Pt-Si.

3. Single Roller Quenching

Work continues on the $\text{Fe}_{80}\text{B}_{20}$ alloy strip, Metglas 2605, produced by Allied Chemical. Additionally, Zr_2Ni metallic glass alloy strip, produced by Phillips Corporation in Eindhoven, The Netherlands, has been investigated as to its structure and stability in the as-received condition as re-splatted in the shock tube splatter. As with the $\text{Fe}_{80}\text{B}_{20}$ the shock tube reduces the amount of as quenched crystallization in the Zr_2Ni .

D. Catalytic Measurements

1. Fischer-Tropsch Reaction

Here we report the near exclusive selectivity of an $\text{Fe}_{80}\text{B}_{20}$ metallic glass catalyst for the production of ethane from the hydrogenation of carbon monoxide. This unusual selectivity arises, we believe, from the equally unique surface structure and composition of the $\text{Fe}_{80}\text{B}_{20}$ alloy metallic glass. The fractal dimension of a model metallic glass surface has been calculated to be 2.3, which indicates a scale of roughness on the atomic dimensions, both in protruberances out of the surface and in the wavelength of the protruberances in the plane of the surface. Thus, such a metallic glass surface appears to be able to achieve high selectivity through steric hindrance of the adsorbing and desorbing molecules. The selectivity for ethane production correlates with the amount of glassy phase present. Conversely, methane production correlates to the level of crystallization of the glassy phase.

Metallic glass catalysts have been observed to have high activity (1, 2) and unusual selectivity (3, 4, 5) in a number of hydrocarbon reactions. In each case, the glassy catalysts were the most selective of hydrogenation over isomerization. Komiyama

have reported about 60% selectivity of ZrNi glass for ethane in the Fischer-Tropsch reaction (6). The results given below show an even higher selectivity for ethane, up to 99%, and a persistence of that selectivity for 20 hours at 320 deg C.

The metallic glasses specimens used in this work were produced by two different techniques. Strip samples were produced by the Allied Chemical Corporation (Metglas 2605) and were used as received. The flake specimens were produced in our shock tube splat cooler by using the 2605 glass as master alloy. Due to the higher cooling rate associated with the shock tube technique, 10^7 °C/sec, as compared to the single roller technique, 10^5 °C/sec, partial crystallinity was present to a far lesser extent in the flake samples than the strip samples, as we will show below.

The Fischer-Tropsch reaction was run in a Pressure Differential Scanning Calorimeter (PDSC) utilized as a flow reactor (7). Use of the PDSC allowed in situ crystallization of the metallic glass and the reevaluation of the catalytic selectivity and activity of the same catalyst by re-running the Fischer-Tropsch reaction over the crystallized glass. Small quantities (5-10 mg) of various catalysts-glasses, crystallized glasses, pure metal foils and powders, and commercial catalysts, were evaluated to allow the comparison between $Fe_{20}B_{80}$ metallic glasses and various forms of crystalline iron catalysts.

Comparisons of Fischer-Tropsch reaction results are given in Figure 29 for ethane selectivity and in Table 5 for several reaction products at a constant 1.5% conversion. As can be seen, some of the glassy FeB shock tube flakes exhibited a 99%

Table 5

FISCHER-TROPSCH REACTION RESULTS (AVERAGE OF N RUNS) AT 320°C.

CATALYST		FISCHER-TROPSCH REACTION RESULTS ¹					ENTHALPY OF CRYSTALLIZATION, $\frac{\text{KJ}}{\text{mole}}$			
Alloy	Form	Nominal Phases	N. # Runs	% Methane	% Ethane	% Propane	Surf. Specific Area, $\frac{\text{m}^2}{\text{gm}}$	Rate, $\frac{\text{mole}}{\text{Lmin m}^2}$	Before F-T Reaction	After Reaction
Fe ₉₀ D ₁₀	Shock Tube Flakes	Glass	2	1	99	-	0.055 ¹	6.9	36	24
Fe ₉₀ D ₁₀	Shock Tube Flakes	Glass	7	75	19	5	0.055 ¹	7.0	10-30	9-16
Fe ₉₀ D ₁₀	Shock Tube Flakes	Crystallized Glass	9	70	24	6	0.055 ¹	6.9	-	-
Fe ₉₀ D ₁₀	Single Roller Strip	Glass	5	77	16	7	0.76 ²	0.6	28	20
Fe ₉₀ D ₁₀	Abraded Single Roller Strip	Glass	5	41	53	6	0.76 ²	0.6	36	28
Fe	Rolled Foil	α -Fe	5	69	24	7	0.01 ³	300	-	-
Fe/graphite	Supported Fe on Graphite	α -Fe	1	77	17	5	2.76 ²	0.2	-	-

1 Measured by BET Kr adsorption

2 Measured by BET N₂ adsorption

3 Calculated geometric surface area

4 1 Atmosphere of 3:1 H₂/CO at a space velocity of 1800 hr⁻¹ at 1.5% conversion

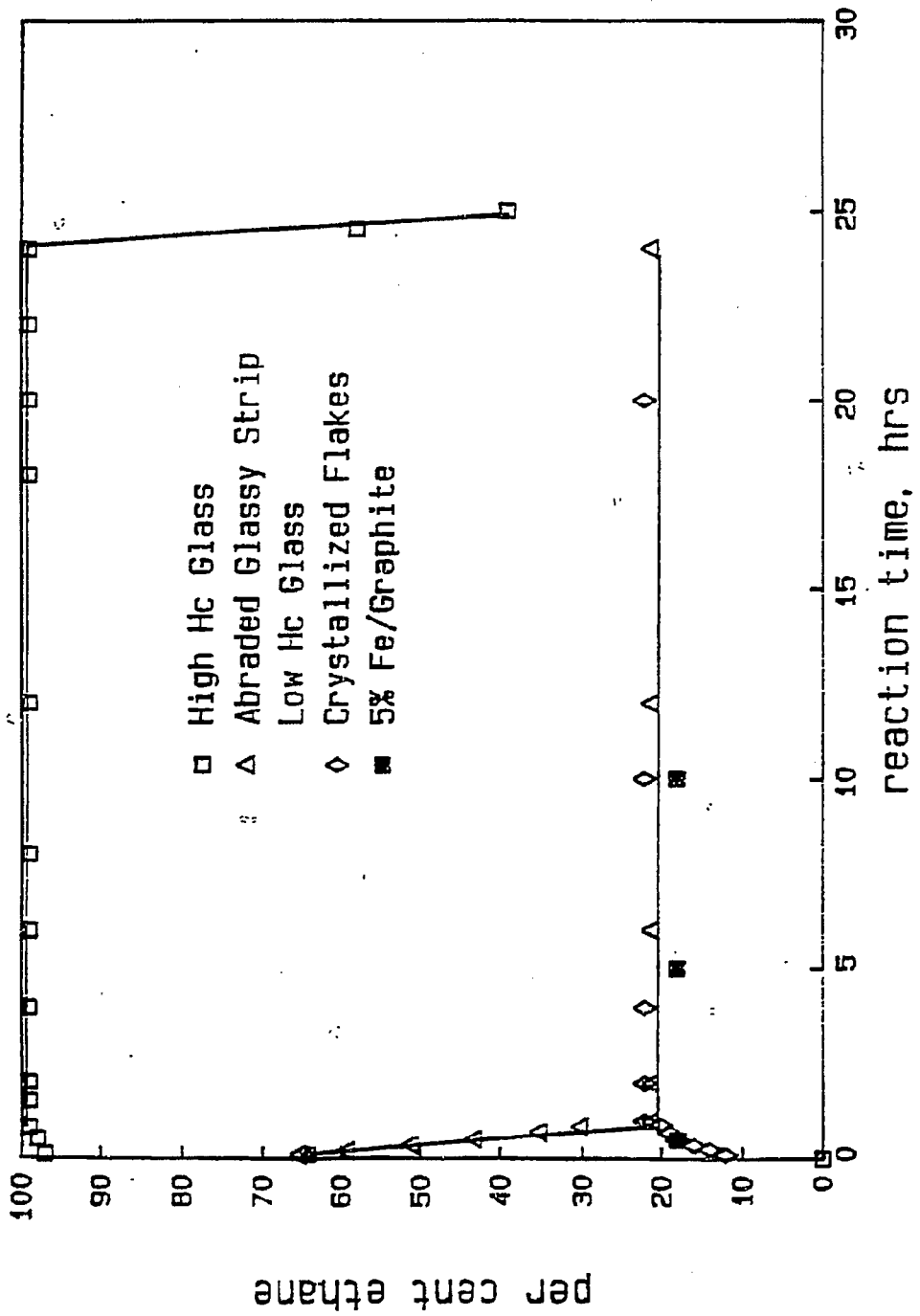


Figure 29
 Time Variation of Ethane Selectivity over
 Fe-Based Catalysts from Table 1

selectivity for ethane, whereas other shock tube flakes showed a selectivity similar to the results over single roller FeB strip, crystallized flakes, Fe foil, and the supported Fe/graphite commercial catalyst. Upon in situ crystallization in He in the PDSC, the ethane selective FeB glass crystallizes with an enthalpy of crystallization, $H = 36$ kcal/mole, much higher than the methane selective FeB flakes and the FeB strip, 10-30 and 28 kcal/mole respectively. However, if the strip of Fe-B glass is abraded heavily, the enthalpy of crystallization increases to 36 kcal/mole. This shift in H correlates to a dramatic shift in selectivity - an increase in the ethane selectivity from 16% to 51% as a result of abrasion. The same flakes that selected 99% ethane, select only 24% ethane after in situ crystallization.

Some of the as-quenched flakes and all of the strip samples show selectivity very similar to the Fe foil and the Fe/graphite catalyst. The similarity of all these selectivities to that of the intentionally crystallized glass indicates the presence of crystallization on the surface and in the bulk of some of the shock tube flakes and all of the single roller strip. Since H of crystallization increases dramatically upon abrasion of the strip, heavy surface crystallization, probably due to atmospheric effects, has occurred, which could be similar behavior to our experiments with cyclohexane (8). The lower H of the abraded Fe-B strip as compared to the most glassy flakes may indicate a higher volume fraction of bulk crystallization in the strip than the more glassy flakes.

Such unique selectivity as exhibited by the metallic glass catalysts surely implies a corresponding uniqueness of the

surface structure of such a glass. The large density of low coordination surface sites on both the glass and the supported metal catalysts indicates at least a partial reason for both types of catalysts' high selectivity for hydrogenation over isomerization (3, 5). However, the selectivity of the metallic glass which we report here is significantly higher for ethane than any previously reported studies on crystalline Fe catalysts (9, 10). A difference which could account for this uniqueness is the lack of neighboring terrace sites on the glassy surface as compared to the ledge and kink sites on the bulk crystalline surface even for small particles. The placement of high coordination number surface sites (active sites according to Falikov and Somorjai (11)) adjacent to low coordination sites is a geometry which does not appear on the small particles. Steric hindrance on the glassy surface may prevent formation of propane and higher hydrocarbons, since the spacing of the next protruberance is 3-4 angstroms for the calculated fractal dimension of 2.3 (12, 13), about the size of n-propane. Such roughness shown in Figure 30, may equivalently cause fast desorption of ethane. We are left with trying to rationalize the remarkable lack of methane production of the glassy surface. If hydrogen is preferentially chemisorbed on terrace sites, the lack of such sites on the proposed model of the metallic glass surface may force hydrogenation via hydrogen adsorbed directly on the chemisorbed carbon atoms, i.e., a Rideal-Eley mechanism rather than the traditional Langmuir-Hinshelwood mechanism for Fischer-Tropsch synthesis. Alternatively, composition wise, the $\text{Fe}_{80}\text{B}_{20}$ glass is a metastable solid solution of B in Fe. The boron

disrupts Fe ensembles on the glassy surface; these ensembles are thought to be required to generate methane (14 - 16). Thus, the glassy surface topology and composition may control the degree of polymerization to a discrete level, in this case to two.

a. References

1. Brower, W. E. Jr., Smith, G. V., Pettit, T. L., and Matyjaszczyk, M. S., *Nature* 301, 497-499 (1983).
2. Smith, G. V., Brower, W. E., Matyjaszczyk, M. S., Pettit, T. L., Proc. 7th Int. Cong. on Catalysis, (Ed. Seiyana, T., Tanabe, K.,) 355 (Elsevier, New York, 1981).
3. Yokoyama, A., Komiyama, H., Inoue, H., Masumoto, T., and Kimura, H. M., *J. Catalysis* 68, 355-361 (1981).
4. Brower, W. E. Jr., Alp, E. E., Kowbel, W., and Simon, K. M., Proc. 8th Int. Cong. on Catalysis, (Verlag Chemie, Berlin, 1984).
5. Smith, G. V., Zahraa, O., Khan, M. M., Richter, B., and Brower, W. E. Jr., *J. Catalyss* 83, 238-241 (1983).
6. Yoshida, H., Fourth Int. Congress on Catalysis, (The Tanaguchi Foundation, Kobe, Japan, 1985).
7. Beecroft, T., Miller, A. W., and Ross, J. R. H., *J. Catalysis* 40, 281-285 (1975).
8. Kowbel, W. and Brower, W. E. Jr., *J. Catalysis* 101, 262-267 (1986).
9. Dwyer, D. J. and Somorjai, G. A., *J. Catalysis* 62, 19-27 (1979).
10. Storch, J. H., Golumbic, N., and Anderson, R. B., *The Fischer-Tropsch and Related Syntheses* (John Wiley, New York, 1951).
11. Somorjai, G. A., *Chemistry in Two Dimensions: Surfaces*, (Cornell Univ. Press, Ithaca, 1981).
12. Kowbel, W. and Brower, W. E. Jr., *J. Non-Crystalline Solids*, in press.
13. Mandelbrodt, B. B., *Fractals: Form, Chance, Dimension*, (W. C. Freeman, San Francisco, 1977).
14. Bouwman, R., Lippits, G. H. M., and Sachtler, W. M. H., *J. Catalysis* 25, 350-355 (1972).

15. Sinfelt, J. H., Catal. Rev. 9, 147-150 (1974).
16. Ponec, V., J. Catalysis 44, 439-445 (1976).

2. Boudouard Reaction

TGA results for CO over a conventional oxide supported nickel catalyst are compared to those over the as-received Zr_2Ni and $Fe_{80}B_{20}$ metallic glasses. Sample sizes for the Dupont 990 system thermogravimetric analyzer experiments were as follows: Ni/SiO₂, Al₂O₃, 18 mg; Zr_2Ni , 5-10 mg; $Fe_{80}B_{20}$, 29 mg. The surface area, S_v , of the supported nickel is assumed to be that observed by van Meerten (16), 325 m²/gm; the S_v of the Zr_2Ni splats is assumed to be that measured by Yokoyama, et al. (9) for $Zr_{65}Pd_{35}$ splats, 0.1 m²/gm; the S_v for the $Fe_{80}B_{20}$ splats is assumed to be that measured by Yokoyama, et al. (5) for the same $Fe_{80}B_{20}$ splats, 0.3 m²/gm.

a. Supported Nickel

The supported nickel was reduced in 30 ml/min. of H₂ at 400°C to reduce surface oxides. Over each of the six supported nickel samples run at various reaction temperatures the weight loss due to H₂ reduction was 14%. After the weight loss due to H₂ cleaning stopped, the H₂ was removed from the system by a 5 ml/min. flow of He. The absence of H₂ in the gas system was confirmed by GC analysis of the gas flow. CO was then admitted at 25 ml/min. at the following temperatures: 280°C, 320°C, 340°C, 380°C and 405°C. Initially CO, CO₂, CH₄ and H₂O were detected at 380°C and 405°C by the Gow-Mac GC utilizing a thermal conductivity detector. At later times, no further CH₄ was detected. At the lower temperatures, no CO₂ or CH₄ and only

Table 6 Dissociation kinetics of CO as measured by thermogravimetric analysis for metallic glasses and a conventional catalyst.

Catalyst	Reaction Temperature °C	Wt. of Catalysts mg	Assumed S_v m^2/cm	m/t mg/min	Rate $cm^3/m^2 \cdot min$
Ni/SiO ₂ , Al ₂ O ₃ (60% Ni)	320	12	325	1.77/70	4.2×10^{-6}
Zr ₂ Ni - metallic glass	322	10	0.1	0.026/50	5.2×10^{-4}
Zr ₂ Ni - metallic glass	250	5.6	0.1	0.022/60	6.5×10^{-4}
Fe ₈₀ B ₂₀ - metallic glass	322	29	0.3	0.057/95	7.0×10^{-5}

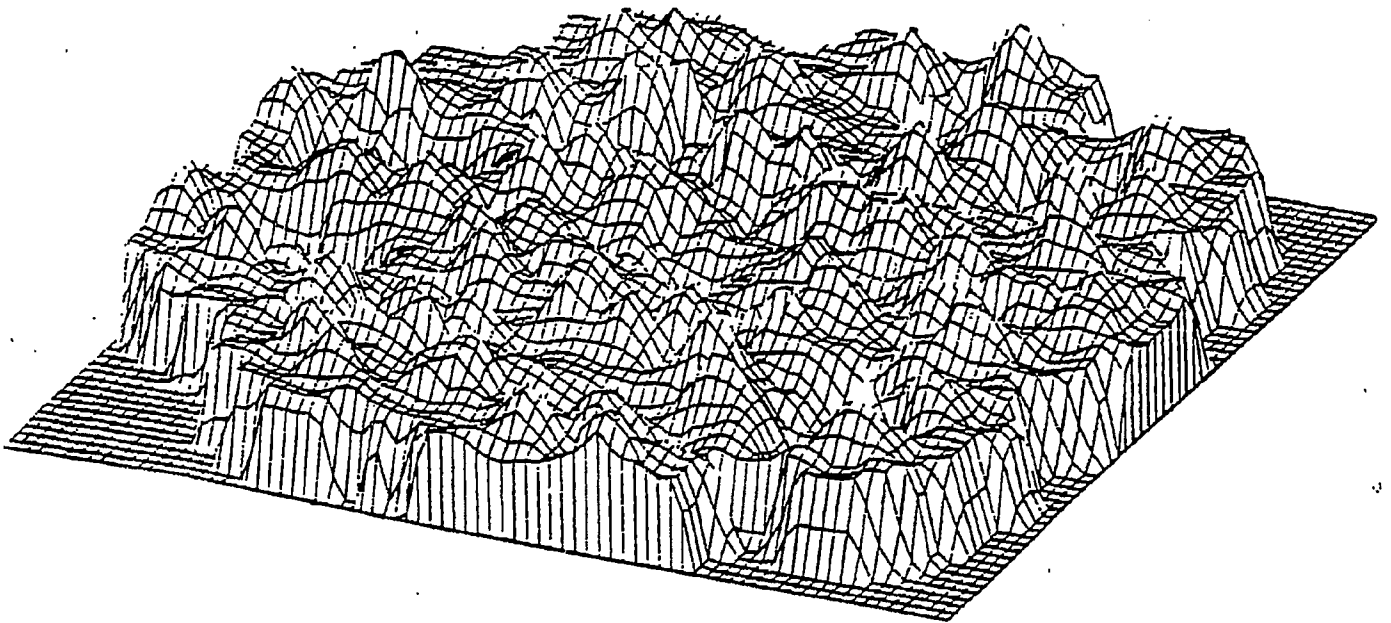


Figure 30 Surface Simulation of Fe-8 Glass Via Trans-section Lines, 2 Lines/Fe Atom.

traces of H₂O were detected. After an initial temperature independent weight gain assumed to be CO adsorption, the average weight gain rates at the five reactions temperatures yielded an average activation energy of 26 kcal/mole.

b. Metallic Glasses

Table 6 shows a comparison of results of weight gains in the TGA after exposure to CO at 322 ± 2°C for the supported nickel catalyst and the Fe₈₀B₂₀ and Zr₂Ni metallic catalysts. Adsorbed and absorbed hydrogen apparently was present in and on the supported nickel after the He flush; the glassy splat strips were exposed only to the He flush to avoid hydride formation. For all the splats, the product gas volumes were off scale for the GC thermal conductivity detector. The mass gains of about 0.002-0.006 mg are near the sensitivity of the TGA - 0.0015 mg. The rate of weight gain per unit surface area (BET determined) for the splats is 10 - 100 times greater than that of the supported nickel.

Measurements in the activity of Pd₄Si and Fe₈₀B₂₀ metallic glasses were carried out in the thermogravimetric analyzer. The rate of weight gain in the presence of a flowing atmosphere of CO was taken as a measure of the rate of deposition of carbon on the catalyst as a result of the dissociation of CO.

c. References

1. Duwez, P., Trans. A. S. M. 60, 605-633 (1967).
2. Brower, W. E., Jr., Matyjaszczyk, M. S., and Pettit, T. L., and Smith, G. V., Nature 301, 497-499 (1983).
3. Smith, G. V., Brower, W. E., Matyjaszczyk, M. E., Pettit, T. L., Proc. 7th Int. Congr. Catalysis (eds. Seiyana, T. and Tanabe, K.,) 355-363 Elsevier, New York 1981.
4. Smith, G. V. Zahraa, O., Khan, M. M., Richter, B., and

- Brower, W. E., Jr., *J. Catal.* (in Press).
5. Yokoyama, A., Komiyama, H., Inoue, H., Masumoto, T., and Kimura, H. M., *J. Catal.* **68**, 355-361 (1981).
 6. Matyjaszczyk, M. S., Ph. D. Dissertation, Southern Illinois Univ., Carbondale (1981).
 7. Greer, A. L., and Leake, J. A. Rapidly Quenched Metals III, Vol. 1, Third Int. Cong., Brighton, 1978.
 8. Yosida, S., Yamashita, H., Funabiki, T., and Yonezawa, T., *J. Soc. Chem. Common.*, 964-965 (1982).
 9. Yokoyama, A., Komiyama, H., Inoue, H., Masumoto, T., and Kimura, H., *Chemistry Letters*, The Chemical Society of Japan, 195-198 (1983).
 10. Vannice, M. A., *Catal. Rev.* **14**, 153 (1976).
 11. Vannice, M. A., *J. Catal.* **37**, 449 (1975).
 12. Dwyer, D. J. and Somorjai, G. A., *J. Catal.* **52**, 291 (1978).
 13. Aruki, M. and Ponec, V., *J. Catal.* **44**, 439, (1976).
 14. Rabo, J. A., Francis, J. N., and Elek, L. F., *Proc. Catal. Congr. Tokyo 1980*.
 15. Alp, E. E., Saporoschenko, M., Simon, K. M., Brower, W. E., Jr., *Proc. Congr. Liquid and Amorphous Metals*, 1983, in press.
 16. Van Meerten, R. Z. C., *New Horizons in Catalysis*, T. Seiyama and K. Tanabe, editors, Elsevier, New York, 1981.
 17. Gaskel, P. H., *Nature* **276**, 484-485 (1978).
 18. Kowbel, W. and Brower, W. E., Jr., in preparation.
 19. Simon, K. M. and Brower, W. E., Jr., submitted to *Metallurgical Transactions A*.
- 3) CHARACTERIZATION OF METALLIC GLASS CATALYSTS WITH THE STERICALLY COMPLEX ORGANIC MOLECULAR PROBE (+)-APOPINENE

a) The Method for Using (+)-Apopinene for Characterizing Surfaces.

We measured the ratio of double bond isomerization to addition, k_i/k_a , for (+)-apopinene during liquid phase hydrogenation conditions at room temperatures and atmospheric pressures on a large number of Pd catalysts and on a smaller

number of Pt catalysts. This ratio was obtained from experimental data from a plot of $\ln(1-2\text{Iso})$ vs. $\ln(1-\text{Add})$ according to the equation

$$\ln(1-2\text{Iso}) = \frac{2k_i}{k_a P_H} \ln(1-\text{Add})$$

derived in our publication describing this method (1). The ratios of k_i/k_a were compared for different catalysts and the differences were interpreted in terms of the kinds of sites thought to catalyze isomerization (edge type) and addition (corner type).

b) Hydrogenation of (+)-Apopinene over Metallic Glasses

(+)-Apopinene was hydrogenated over glassy (amorphous) and crystalline Pd-Si and Pd-Ge alloys as well as over splat cooled pure Pd, Pd foil, and Pt foil. The catalysts are differentiated from each other by their differing abilities to catalyze isomerization and addition of (+)-apopinene. Heat treatment of the rapidly cooled alloys results in relative increases in isomerization activity over addition activity which is interpreted as surface structural changes. Such changes do not occur for the rapidly cooled pure Pd. The results are interpreted to indicate that the glassy surfaces contain many sites of high coordinative unsaturation (protuberances) with few nearest neighbors while the crystalline surfaces resulting from heating the former contain fewer such sites but more sites of relative lower coordinative unsaturation. Thus, the data favor a glassy surface structure which is not two-dimensionally random (flat), but is three-dimensionally random (hilly or rolling). Therefore, the glassy surface does not appear to crystallize into

terraces, as it would if it were flat, but to crystallize into staircases of steps and kinks because it contains many protuberances. (2,3)

Additionally, the selectivities for half-hydrogenation of phenylacetylene, 1-octyne, and 4-octyne were examined over Pd-Si and Pd-Ge glassy (amorphous) and crystalline catalysts and, for comparison, over splat cooled pure Pd, reduced PdO₂, Pd foil, Pt foil, Pd/Al₂O₃, and Pd/C. Only the Pd/C and Pt foil gave less than 90% selectivities. Terminal alkynes comminute Pd structures and expose new active sites. These new sites are different on the rapidly cooled catalysts and the regularly crystallized catalysts. Although no significant changes are detected in alkyne hydrogenation selectivities after several hydrogenations, significant changes are revealed by (+)-apopinene. On the terminal acetylene-treated foils and on the reduced Pd oxide the rates of addition and isomerization of (+)-apopinene increase, but the ratio of the two rates remain almost the same. In contrast, the splat cooled catalysts show a higher rate increase for isomerization than for addition. (4)

c) The Characterization of Pt Catalysts with (+)-Apopinene

Six Pt/SiO₂ and four Pt/Al₂O₃ catalysts were characterized by CO chemisorption and H₂-O₂ titration and by electron microscopy. Five of the Pt/SiO₂ catalysts originated at Northwestern University and had been similarly characterized before. Over these catalysts the hydrogenation reaction of (+)-apopinene was used to evaluate the change in the mix of active sites as a function of percent exposed Pt atoms (percent dispersion, %D). The ratio of isomerization to addition, k_i/k_a ,

goes through a maximum at approximately 60%D, which corresponds to a maximum in edge sites (C_7 sites) on fcc octahedra. These sites are identified as Siegel type 2M sites which catalyze essentially isomerization whereas adatoms and vertices (C_4 sites), Siegel type 3M sites, catalyze addition and isomerization.(5)

d) The Characterization of Pd Catalysts with (+)-Apopinene

A series of fourteen supported palladium catalysts ranging in percent exposed palladium atoms (percent dispersion, %D) from 16.7% to 100% have been examined with the hydrogenation reaction of (+)-apopinene. The ratio of isomerization to addition, k_i/k_a , goes through a maximum at approximately 60 %D, a maximum which is found also for supported Pt catalysts. This maximum occurs approximately at the maximum in the number of edge sites for fcc truncated octahedral crystallites as a function of %D. Based on the data a scale of percent edge character is derived.(6)

e) References

1. G. V. Smith, A. Molnár, M. M., Khan, D. Ostgard, N. Yoshida, "Characterization of Palladium Surfaces with (+)-Apopinene: Correlation of Reaction Path with Surface Features", Journal of Catalysis, 98 (1986) 502-512.
2. A. Molnár, G. V., Smith, M., Bartók, "Hydrogenation of (+)-Apopinene over Pd-Si and Pd-Ge Glasses", Journal of Catalysis, 101 1986 540-544.
3. G. V. Smith, O. Zahraa, M. Khan, B. Richter, and W. E. Brower, Jr., "Characterization of Pd-On-Alumina and Pd-Si Glasses by Isomerization and Hydrogenation of (+) - Apopinene", Journal of Catalysis, 83, 238-241 (1983).
4. A. Molnár, G. V. Smith, M., Bartók, "Selective Hydrogenation of Alkyenes over Metallic Glasses", Journal of Catalysis, 101 1986 67-77.
5. F. Notheisz, M. Bartók, D. Ostgard, G. V., Smith, "Hydrogenation and Isomerization of (+)-Apopinene over

well Characterized Pt/SiO₂", Journal of Catalysis, 101
1986 212-217.

6. G. V. Smith, D. Ostgard, M. Bartók, and F. Notheisz, "Hydrogenation and Isomerization of (+)-Apopinene on Pd Catalysts", accepted for publication in the Proceedings of the 11th Biennial Meeting of the Organic Reaction Catalysis Society, Savannah Georgia, April 7-9, 1986.

E. Publications and Presentation

1. Publications

1. G. V. Smith, W. E. Brower, Jr., M. Matyjaszczyk, and T. Pettit, "Metallic Glasses: New Catalytic Systems for Hydrogen Reactions", Proceedings of the Seventh International Congress on Catalysis, July, 1980, published in New Horizons in Catalysis, Ed. T. Seiyana, Elsevier, New York, 1981.
2. S. D. Bader, L. Richter, M. B. Brodsky, W. E. Brower, Jr. and G. V. Smith, "Silicon L₂₃ vv Auger Lineshape and Oxygen Chemisorption Study of Pd₄Si", Solid State Communications, 37 (1981), 729.
3. W. E. Brower, Jr., M. S. Matyjaszczyk, T. L. Pettit, and G. V. Smith, "Metallic Glasses as Novel Catalysts", Nature, 301 (1983), 497-499.
4. G. V. Smith, O. Zahraa, M. Khan, B. Richter, and W. E. Brower, Jr., "Characterization of Pd-On-Alumina and Pd-Si Glasses by Isomerization and Hydrogenation of (+)-Apopinene", Journal of Catalysis, 83, 238-241 (1983).
5. E. E. Alp, K. M. Simon, M. Saporoshenko and W. E. Brower, Jr., "Moessbauer and DTA Measurements on Fe₈₀B Metallic Glasses", J. Noncrystalline Solids, 61 and 62, pp. 871-876, 1984.
6. W. E. Brower, Jr., E. E. Alp, W. Kowbel and K. M. Simon, "Evaluation of the Catalytic Behavior of Metallic Glass Via Thermal Analysis, Moessbauer Spectroscopy and Electron Microscopy" 8th Int. Congress on Catalysis, Verlag Chemie, Berlin, 1984.
7. E. E. Alp, M. Saporoshenko, and W. E. Brower, Jr., "Location of Crystallization in Fe₈₀B₂₀ Metallic Glass by CEMS", 5th Int. Congress on Rapidly Quenched Metals, Wurtzberg, West Germany, 1984.
8. K. M. Simon and W. E. Brower, Jr. "Crystallization of Zn₂Ni Metallic Glass", Met. Trans. Accepted for Publication.

9. S. C. Megli, D. L. Eddingfield, and W. E. Brower, Jr.
"Heat and Fluid Flow During the Formation of Pd₈₀Si₂₀
Metallic Glasses, Met. Trans. Accepted for publication.
 10. W. Kowbel and W. E. Brower, Jr., "In Situ HVEM
Observations of the Effect of Chemisorption on
Crystallization of Pd₄Si Metallic Glass", J. Catalysis,
101, (1986) 262-267.
 11. S. Overbury, D. Huntley, and W. E. Brower, Jr., "Low
Angle Ion Scattering Studies of the Surface Structure of
Fe₄B Metallic Glass", Applied Surface Science, 27
(1986) 1980-198.
 12. G. V. Smith, A. Molnar, M. M., Khan, D. Ostgard,
N. Yoshida, "Characterization of Palladium Surfaces with
(+)-Apopinene: Correlation of Reaction Path with Surface
Features", Journal of Catalysis, 98 (1986) 502-512.
 13. A. Molnar, G. V., Smith, M., Bartók,
"Hydrogenation of (+)-Apopinene over Pd-Si and Pd-Ge
Glasses", Journal of Catalysis, 101 1986 540-544.
 14. A. Molnar, G. V. Smith, M., Bartók, "Selective
Hydrogenation of Alkenes over Metallic Glasses", Journal
of Catalysis, 101 1986 67-77.
 15. F. Notheisz, M. Bartók, D. Ostgard, G. V., Smith,
"Hydrogenation and Isomerization of (+)-Apopinene over
well Characterized Pt/SiO₂", Journal of Catalysis, 101
1986 212-217.
2. In Press - preprints enclosed
1. W. Kowbel and W. E. Brower, Jr. "Surface Structural Model
of a Metallic Glass", accepted, J. Noncrystalline Solids.
 2. G. V. Smith, D. Ostgard, M. Bartók, and F. Notheisz,
"Hydrogenation and Isomerization of (+)-Apopinene on Pd
Catalysts".
3. Presentations
1. G. V. Smith, W. E. Brower, Jr., M. Matyjaszczyk, and T.
Pettit. "Metallic Glasses and Extended Solid Solutions as
New Catalysts Systems", Annual Meeting of the North
American Catalysis Soc., Boston, 1981.
 2. W. E. Brower, Jr., M. Matyjaszczyk, and G. V. Smith.
"Catalyst Artificial Rhodium as a Testing Material for
the Horvoti Polangi Mechanism of Hydrogenations
Reactions", AIChE Annual Meeting, Dallas, 1982.
 3. W. E. Brower, Jr. and G. V. Smith. "Alkenes as Molecular
Probes of Metallic Glass Catalyst Surfaces", AIChE Annual
Meeting Dallas, 1982.

4. W. E. Brower, Jr. "Metallic Glass Catalysts", Gordon Conference on Catalysis, New London, NH, 1983.
5. W. E. Brower, Jr., E. E. Alp, W. Kowbel, and K. M. Simon. "Evaluation of Catalytic Behavior of Metallic Glasses Via Thermal Analysis, Moessbauer Spectroscopy and Electron Microscopy, 8th Int. Congress on Catalysis, Berlin, 1984.
6. W. E. Brower, Jr., S. Karoglianian, and S. C. Megli. "Heat and Fluid Flow During Metallic Glass Formation", AIME Annual Meeting, Detroit, 1984.
7. W. E. Brower, Jr. "Stability of the Selectivity of Metallic Glass Catalysts:", Annual Meeting of the Materials Research Society, Boston, 1984.
8. W. E. Brower, Jr., W. Kowbel, P. Tlomak, and C. Irons, "Catalytic Activity and Selectivity of Metallic Glasses in Hydrogen Reactions", AIME Annual Meeting, Toronto, Canada, 1985.
9. W. E. Brower, Jr., "Amorphous Metal Alloys - A Rough Route to Selectivity", 4th International Conference on Catalysis, Osaka, Japan, 1985.
10. W. E. Brower, Jr., P. Tlomak, W. Kowbel, S. J. Pierz, "The Nature of the Surface of a Metal-Metalloid Glass", Proceedings of Symposium on Characterization of Defects in Materials, Materials Research Society, 1986.
11. W. E. Brower, Jr., W. Kowbel, and P. Tlomak, "Correlation of the Crystallization of a Metallic Glass With Its Catalytic Selectivity", Proceedings of Symposium on Rapidly Quenched Alloys, Materials Research Society, 1986.
12. W. E. Brower, Jr., W. Kowbel, and P. Tlomak, "Unusual Selectivity for Ethane in the Fischer-Tropsch Reaction With an Iron-Boron Metallic Glass Catalyst", in preparation.
13. G. V. Smith, "Metallic Glasses as New Catalyst Systems for Energy Conversion", Washington, DC, May 6-7, 1981.
14. G. V. Smith, "Metallic Glasses in Hydrogenation", Welch Foundation, Houston, TX, November 6-11, 1981.
15. G. V. Smith, "Molecular Probes in Catalysis", Abilene Christian College, Abilene, TX, November 24, 1981.
16. G. V. Smith, A. Molnár, M. M. Khan, B. Rihter, W. Kowbel, and W. E. Brower, Jr., "(+)Apopinene as a Molecular Probe for the Characterization of Glassy and Crystalline Palladium Surfaces", ACS Meeting, Seattle, WA, March 23, 1983.

17. G. V. Smith, W. E. Brower, Jr., A. Molnár, M. Khan, B. Rihter, and W. Kowbel, "Characterization of Pd-on-Alumina and Pd-Si Glasses by Isomerization and Hydrogenation of (+)Apopinene", Eighth North American Meeting of the Catalysis Society, Philadelphia, PA, May 4, 1983.
18. G. V. Smith, "Hydrogenation, Deuterium Exchange, Isomerization, and Racemization of Molecular Surface Probes for the characterization of Metal Catalysts", Eastern Regional Research Center, US Department of Agriculture, Philadelphia, PA, May 5, 1983.
19. G. V. Smith, "Characterization of Metal Surfaces with (+)Apopinene", Dow Chemical Company, Midland, MI, August 15, 1983.
20. G. V. Smith, "Hydrogenation and Exchange of Alkenes over Supported Metal Catalysts", Department of Organic Chemistry, Szeged, Hungary, January 15, 1985.
21. G. V. Smith, "Characterization of Highly Dispersed Metal Catalysts", IX North American Meeting of The Catalysis Society, Houston, TX, March 17-21, 1985.
22. G. V. Smith, "Characterization of Highly Dispersed Metal Catalysts", Department of Chemistry, University of California, Berkeley, April 26, 1985.
23. G. V. Smith, "Characterization of Highly Dispersed Metal Catalysts", Signal Research, Des Plaines, IL, May 30, 1985.
24. G. V. Smith, "Characterization of Highly Dispersed Metal Catalysts", AMOCO Oil Co., Harvey, IL, June, 26, 1985.
25. G. V. Smith, F. Notheisz, D. Ostgard, and M. Bartók, "Characterization of Highly Dispersed Supported Palladium Catalysts with (+)-Apopinene, 20th Great Lakes Regional ACS, Keith Hall Symposium, Milwaukee, WI, June 2-3, 1986.
26. G. V. Smith, F. Notheisz, D. Ostgard, and M. Bartók, "Characterization of Highly Dispersed Supported Palladium Catalysts with (+)-Apopinene", VIth International Conference of Organic Synthesis, Moscow, USSR, August 10-15, 1986.
27. G. V. Smith, F. Notheisz, D. Ostgard, and M. Bartók, "Hydrogenation and Isomerization of (+)-Apopinene on Pd Catalysts, Eleventh Conference Catalysis of Organic Reaction, Savannah, GA, April 7-9, 1986.

28. G. V. Smith, F. Notheisz, D. Ostgard, and M. Bartók, "Characterization of Highly Dispersed Supported Palladium Catalysts with (+)-Apopinene", University of Missouri, St. Louis, MO, September, 29, 1986.
29. G. V. Smith, "Characterization of Highly Dispersed Supported Palladium Catalysts with (+)-Apopinene", Catalysis Club of Chicago Spring Symposium, May 12, 1986.

G. Theses

Five M.S. theses were completed by S. C. Megli, K. M. Simon, and S. Karoglanian, graduate students in Engineering and T. Pettit and Z. Ali in Chemistry. Mr. Megli's thesis was completed in May 1983, and was a model of the heat and fluid flow during splat cooling for two sided, hammer and anvil type splat cooling. Variations of superheat and hammer velocity were compared for $Pd_{80}Si_{20}$ and $Fe_{80}B_{20}$ metallic glasses. The model calculations showed that the fluid flow is essentially complete before cooling begins. Experimentally determined variations of splat thicknesses versus superheat and hammer speed were in agreement with the model predictions. This work has been accepted for publication in Metallurgical Transactions A. Mr. Simon's thesis concerned characterization of metallic glasses as to their structure, stability, and activity in the dissociation of CO. A manuscript concerning the structure and stability of Zr_2Ni metallic glass has been accepted for publication in Metallurgical Transactions A. Mr. Simon's work is also part of the work presented in the paper presented at the Eighth International Congress on Catalysis. Mr. Karoglanian's work on supersonic nozzle splat cooler design was presented at the annual meeting of AIME. Mr. Pettit performed the first catalytic studies on metallic glasses. Ms. Ali measured the heat of hydrogenation of (+)-apopinene.

H. Dissertations

1. M. Matyjaszczyk, "Metallic Glasses as Catalysts", 1982.
2. E. E. Alp, "The Structure and the Thermal Stability of $\text{Fe}_{80}\text{B}_{20}$ Metallic Glass by Moessbauer Spectroscopy", 1984.
3. W. Kowbel, "Modelling and Experimental Characterization of the Surface Structure of $\text{Pd}_{80}\text{Si}_{20}$ and $\text{Fe}_{80}\text{B}_{20}$ Metallic Glasses", 1985.
4. M. Khan, "Effects of Solvent and Surface Structure on Catalytic Hydrogenation of Olefins", 1983.
5. B. Rihter, "Syntheses and Isomerization of Deuterated Apopinenes over Palladium Catalysts", 1985.

I. Personnel

1. Research Associates

Dr. A. D. van Langeveld has worked on the project working with Dr. Brower from 11/1/83 to 5/15/84. He graduated from Prof Vladmier Ponec's group in Leiden, The Netherlands, and is presently with Phillips Corp in Eindhoven.

Dr. Noritetsu Yoshida worked in Dr. Smith's laboratory from December 1982 thru March 1984 while on leave from the Department of Chemistry, Kobe University, where he is an Assistant Professor. He holds a Doctor of Science degree in Physical Chemistry from Alaska University.

Dr. Árpád Molnár an Associate Professor at Jozsef Attila University in Szeged Hungary worked with Dr. Smith from June 1982 thru August 1983. He is with the research group of Professor M. Bartók. There is an active collaboration between the laboratories of Professors Bartok and Smith thru an agreement between the National Science Foundation and the Hungarian Academy of Science.

Dr. Ferenc Notheisz of József Attila University worked at SIU-C from July 1983 thru September 1984. He received his Ph.D. in 1970.

Also, from József Attila University, Dr. Agnes Gregus worked in Dr. Smith's laboratory from August 1984 thru October 1985. She received her degree in 1980.

The most recent researcher to work in Dr. Smith's laboratory thru the collaboration with Professor Bartók was Mr. István Pálincó. He was employed at SIU-C from November 1985 thru October 1986. He received his University diploma in June 1983.

2. Ph.D. Students

Four Ph.D. students (three in Molecular Science and one in Engineering) that work with Dr. Brower have contributed to the project, Maciej Matyjaszczyk, Witold Kowbel, Ercan Alp and Pawel Tlomak (Ph.D. in progress).

Five Ph.D. students (in Chemistry) that work with Dr. Smith have contributed to the project, Muhib Khan and Boris Rihter (Ph.D.s completed), Daniel Ostgard, Parfait Likibi, and Rouzhi Song (Ph.D.s in progress).

3. M.S. Students

Three M.S. students, working with Dr. Brower, Kirk Simon, Steven Megli, and Serop Karoglanian have contributed to the project.

Three M.S. students, working with Dr. Smith, Thomas Pettit, Zawiah Ali (degrees completed), and Sariwan Tjandra have contributed to the project.